FRACTURE MECHANICS OF FUNCTIONALLY GRADED MATERIALS

Final Technical Report

F. Erdogan

Lehigh University
Bethlehem, PA 18015

October 1996

Prepared for

U.S. Air Force Office of Scientific Research

Grant No. F49620-93-1-0252

REPORT DOCUMENTATION PAGE

Form Approved
OMB No. 0704-0188

1. AGENCY USE ONLY *(Leave blank)*

2. REPORT DATE

3. REPORT TYPE AND DATES COVERED
FINAL 4/1/93-8/31/96

4. TITLE AND SUBTITLE
"Fracture Mechanics of Functionally Graded Materials"

5. FUNDING NUMBERS
AFOSR
F49620-93-1-0252
Grant

6. AUTHOR(S)
Dr. Fazil Erdogan

7. PERFORMING ORGANIZATION NAME(S) AND ADDRESS(ES)
Lehigh University
19 Memorial Drive West
Bethlehem, PA 18015

8. PERFORMING ORGANIZATION REPORT NUMBER
533033

9. SPONSORING/MONITORING AGENCY NAME(S) AND ADDRESS(ES)
Air Force Office of Scientific Research
110 Duncan Avenue, Suite B115
Bolling AFB, DC 20332

10. SPONSORING/MONITORING AGENCY REPORT NUMBER

11. SUPPLEMENTARY NOTES
Most of the significant results obtained during the course of this research have been reported in eleven manuscripts which have been published in or accepted for publication by various journals. The technical monitor of this research project was Dr. Walter F. Jones, AFOSR, Bolling Air Force Base, DC 20332-0001.

12a. DISTRIBUTION/AVAILABILITY STATEMENT
Approved for public release;
distribution unlimited.

12b. DISTRIBUTION CODE

13. ABSTRACT *(Maximum 200 words)*
Functionally graded materials are generally two-phase composites with continuously varying volume fractions. Used as coatings and interfacial zones, they help to reduce mechanically and thermally induced stresses caused by the material property mismatch and improve the bonding strength. In this project some basic problems concerning fracture mechanics of graded materials are identified, general analytical methods for solving the related crack problems are developed, the singular behavior of the solutions for typical material nonhomogeneities is examined, and solutions of some benchmark problems are obtained. The results are intended to provide technical support for material scientists and engineers who are trying to develop methods for processing these materials and for design engineers who are interested in using them in technological applications. Typical applications of functionally graded materials include thermal barrier coatings of high temperature components in gas turbines, surface hardening for tribological profection, and as interlayers in microelectronic and optoelectronic components.

14. SUBJECT TERMS
Functionally graded materials; fracture mechanics; surface cracking; graded coatings; graded interfacial zones; debonding; thermal barrier coatings

15. NUMBER OF PAGES

16. PRICE CODE

17. SECURITY CLASSIFICATION OF REPORT	18. SECURITY CLASSIFICATION OF THIS PAGE	19. SECURITY CLASSIFICATION OF ABSTRACT	20. LIMITATION OF ABSTRACT
Unclassified	Unclassified	Unclassified	Unlimited

FRACTURE MECHANICS OF FUNCTIONALLY GRADED MATERIALS

Final Technical Report

F. Erdogan

Lehigh University
Bethlehem, PA 18015

October 1996

Prepared for

U.S. Air Force Office of Scientific Research

Grant No. F49620-93-1-0252

TABLE OF CONTENTS

FRACTURE MECHANICS OF FUNCTIONALLY GRADED MATERIALS

ABSTRACT

Functionally graded materials are generally two-phase composites with continuously varying volume fractions. Used as coatings and interfacial zones, they help to reduce mechanically and thermally induced stresses caused by the material property mismatch and to improve the bonding strength. In this project some basic problems concerning fracture mechanics of graded materials are identified, general analytical methods for solving the related crack problems are developed, the singular behavior of the solutions for typical material nonhomogeneities is examined, and solutions of some benchmark problems are obtained. The results are intended to provide technical support for material scientists and engineers who are trying to develop methods for processing these materials and for design engineers who are interested in using them in technological applications. Typical applications of functionally graded materials include thermal barrier coatings of high temperature components in gas turbines, surface hardening for tribological protection, and as interlayers in microelectronic and optoelectronic components.

The results found show that by eliminating the discontinuities in material property distributions the mathemaitcal anomalies regarding the crack tip stress oscillations for the interface cracks and the nonsquare-root singularities for cracks intersecting the interfaces are also eliminated. From the viewpoint of fracture mechanics the importance of this result lies in the fact that in analyzing the components involving functionally graded materials one can use the existing crack tip finite element modeling developed for ordinary square-root singularities and apply the energy balance-based theories of conventional fracture mechanics. The benchmark problems considered in this project are concerned primarily with surface cracking and debonding.

1. INTRODUCTION TO FUNCTIONALLY GRADED MATERIALS

To meet the expected stringent demands of future technologies in power generation, transportation, aerospace, and microelectronics, in current research a greater emphasis will have to be placed on material design, more specifically, on developing new materials or material systems tailored for specific applications. Generally such materials tend to be composites and intermetallics having homogeneous bulk properties. The composites may be fiber or filament reinforced, particulate, or layered in structure. Many of the laminated materials, thin films and coatings fall into the latter category. A common feature of composites is that they consist of bonded dissimilar homogeneous materials. Consequently, in studying mechanics, particularly failure mechanics of such materials the nature of interfaces or interfacial regions would play an extremely important role. From a mechanics view point, material property discontinuities across the interfaces would have generally two undesirable consequences, namely higher residual, thermal and mechanical stresses, and weaker bonding strength. To circumvent these difficulties, very often the interfacial regions are modified by intorducing a third medium in the form of an *interlayer*, mechanically roughening the surfaces, or using coupling agents.

An alternative concept which may also be used to overcome some of the shortcomings of piecewise homogeneous materials, particularly of layered dissimilar materials, would be the introduction of interfacial regions or coatings with *graded* thermomechanical properties(*) [1]-[7]. Thus, by varying the volume fractions of the constituents between zero to one hundred percent, thereby obtaining a continuous through-thickness material property variation, it is possible to obtain not only smoother stress distributions and lower stress concentrations [8*], [9], but also higher bonding strength [10]. For example, in [8*] it was shown that the point of intersection of the free end and the interface between a homogeneous coating and the substrate is a point of stress singularity and, consequently, a potential location of debonding crack initiation.

(*) Numbers in brackets refer to the references listed in Section 4 of this report. The references marked by an (*) describe research which is fully or partly supported by the current AFOSR grant.

On the other hand, if the homogeneous coating is replaced by a graded layer, the singularity disappears and the stress distribution becomes considerably smoother.

In many of the deposition and bonding processes used in ceramic coatings, it is difficult to obtain the desired strength for the interfacial region. This is due largely to poor adhesion and partly to high stress concentrations. The adverse influence of both of these factors can be reduced significantly by introducing a graded interfacial zone between the two materials. The technique can be particularly useful for material pairs in which the bonding is inherently difficult. for example, in [10] it was shown that for a diamond film synthesized over a 50/50 W/Mo alloy by using a DC plasma jet, the measured bonding strength is less than 10 kg/cm^2. On the other hand, if a graded interfacial zone is introduced by first plasma-spraying the substrate with tungsten carbide and then gradually adding increasing amounts of methane and hydrogen before growing the diamond film, the adhesive strength is measured to be over 150 kg/cm^2.

These particulate composites with continuously varying volume fractions are called *functionally graded materials* (FGM). By controlling not only the composition of profile but also the microstructure, the concept of FGM's could provide a great deal of flexibility in material design. As the processing techniques improve, the potential for special applications of FGM's appears to be nearly unlimited. However, in the immediate future the primary use of these new materials will most likely be limited to thermal barrier coatings, wear-resistant coatings and corrosion-resistant coatings [11].

1.1 Thermal Barrier Coatings

Within the past decade or so considerable progress has been made in using ceramic coatings to protect metallic components from high temperature turbine environments. These *thermal barrier coatings* (TBC's) are currently being used in conjunction with air cooling to prolong the life of hot-section turbine components in aircraft engines. The application of TBC's also offers the possibility of increasing the thermodynamic efficiency of land-based turbines by increasing the inlet temperature of gases. Thus, the TBC technology is considered by many as a viable means for developing more efficient aircraft engines and stationary gas turbines. There are,

however, several major technical issues involving the next generation of TBC's, namely (i) improvements in processing techniques from both economic and performance standpoints, (ii) understanding the failure mechanisms of TBC's in simulated and actual turbine environments, and (iii) developing characterization and test methodologies to measure time and temperature-dependent characteristics of TBC's for reliable life prediction.

The current approach for accommodating the material property mismatch between the ceramic coating and metallic substrate is to make the ceramic layer to be more compliant (or "strain tolerant") by introducing defects such as microcracks, porosity and segmented columnar microstructure. The difficulty with this solution is that the particular microstructural features that provide compliant coatings also provide rapid diffusion paths for oxygen. The experience seems to indicate that by far the most critical factor limiting the performance of the state-of-the-art TBC's is the spallation of the ceramic layer which takes place either along a plane parallel to the ceramic-bond coat interface (as in plasma-spray coatings), or along the interface between the bond coat and its oxide scale (usually Al_2O_3) (as in coatings processed by using electron beam physical vapor deposition). In both cases the life of the coating is controlled by the oxidation time and the number of thermal cycles.

The basic conjecture behind the FGM concept is that by replacing sharp interfaces with graded interfacial zones or by replacing homogeneous ceramic layers with metal/ceramic FGM's, it is possible to improve the resistance of the coating to spallation as a result of reduced stress levels and improved bonding strength.

1.2 Wear-Resistant Coatings/Abradable Seals

One obvious application of ceramic coatings apears to be to provide the necessary hardness or wear resistance to the surfaces of structural components transmitting forces through contact, such as gears, bearings, cams and machine tools. Intuitively it is clear that the fatigue life of these components may be improved quite considerably if one uses a graded rather than a homogeneous ceramic coating on the metallic substrate. In these

load-transfer components FGM coatings would provide the necessary surface hardness without sacrificing the overall toughness.

A related application of the FGM interfacial zones or coatings may be found in the abradable seals used in some stationary gas turbines to help minimize the gas leakage through the gap between the tips of rotating blades and the turbine shroud. The problem is again a contact problem and the primary material property requirements are abradability and toughness. The main components in the shroud are the metallic structure or the substrate, bond coat, high density ceramic and very low density ceramic with a graded zone replacing every sharp interface [11].

In the past wear and corrosion-resistant coatings have been used quite extensively in industrial machinery. The coating material has been metals such as stainless steels, Mo-based alloys and WC-Co as well as ceramics such as Al_2O_3-TiO_2 and Cr_2O_3. For example, WC-Co and Cr_3C_2 / NiCr have been extensively used in aircraft industry to coat various turbine/compressor components and mid-span stiffeners for improved wear-resistance. Other applications of wear-resistant coatings have been in printing rolls, steel mills, petrochemical industry, and automobile industry. Most of these coatings have been deposited by using a thermal spray process. Since thermal spray technique is readily suitable for grading the composition of the coating, service life improvements can be obtained in all applications of wear-resistant coatings by using the FGM concept.

1.3 Oxidation-Resistant Coatings

The main desirable characteristics of an ideal TBC appear to be low conductivity for thermal insulation, high coefficient of thermal expansion to match that of the metallic substrate, and high resistance to oxygen diffusion. It is highly unlikely to find all these favorable properties in a single material. Many of the well known ceramics have either high conductivity and low oxygen diffusivity or low conductivity and high oxygen diffusivity. to prevent oxygen diffusion at some point a layer of Al_2O_3 or mullite ($Al_2O_3 \bullet 2SiO_2$) may be needed. However, these materials have considerably higher thermal conductivity than that of, for example, YSZ (ytria-stabilized zirconia). Thus, the

problem appears to be an optimal design of a multi-layered structure, including graded interfacial zones and coatings.

Typically, the current design of TBC's consists of a partially stabilized zirconia coating deposited on an intermediate metallic bond coat (e.g., NiCr AlY) which is plasma sprayed on the (superalloy) substrate [7]. the main function of the bond coat is to protect the substrate against oxidation. It also helps to reduce thermal expansion mismatch between the ceramic coating and the metallic substrate, and provides surface texture to improve bonding. At high temperatures an oxide (Al_2O_3) scale is formed along the PSZ-bond coat interface. Even though this Al_2O_3 layer forms an oxygen diffusion barrier, it also introduces a weak cleavage plane which, under thermal cycling, may lead to spallation. This difficulty may be overcome by introducing a graded (NiCrAl_2Y-PSZ) layer between the bond coat and the ceramic layer [7].

2. OBJECTIVES OF THE RESEARCH PROGRAM

The objectives of the research program supported by the AFOSR Grant have been

- To identify some basic problems concerning the *fracture mechanics of functionally graded materials.*
- To develop general methods for solving the related crack problems.
- To examine the singular behavior of the solutions of the crack problems in FGM's and compare them with the corresponding results in homogeneous and piecewise homogeneous materials.
- To obtain solutions for some benchmark problems.

In general, the results of the research program are intended *to provide technical support for material scientists and engineers who are trying to develop methods for processing FGMs and for design engineers who are interested in applications.* Specifically, the *crack tip singularities* found and the *benchmark solutions* provided would be quite useful in the development and testing of finite element moldes for solving more complex problems involving FGMs.

3. FRACTURE MECHANICS OF GRADED MATERIALS - STRESS SINGULARITIES AND BENCHMARK SOLUTIONS

In this section, after describing some elementary concepts of *fracture mechanics*, a brief discussion of the topic as it relates to the graded materials is presented. Stress singularities for each typical crack geometry are then examined and sample results obtained from a series of benchmark solutions are discussed. the analytical details and more extensive results are given in References [8*] and [12*]-[20*].

3.1 Fracture Mechanics - Elementary Concepts

In a broad sense "fracture" is creation of new surfaces in solids. The macroscopic theories of fracture are based on the notions of continuum mechanics and classical thermodynamics. In studying the subject, it is implicitly assumed that the material contains some macroscopic flaws and the medium is homogeneous in the sense that the size of these flaws is large compared to the characteristic microstructural dimension of the materials. The problem is to study the effect of the applied loads, flaw geometry and the environmental conditions on the fracture of the solid - a subject which has come to be known as *fracture mechanics*. The fundamental criterion of fracture initiation and propagation is based on the energy balance concept. Let the solid contain a dominant flaw which is usually considered to be a planar crack of surface area A. Under given external loads if the crack grows by an amount dA in time dt, the thermodynamic equilibrium of the solid requires that

$$\frac{dU}{dt} = \frac{dV}{dt} + \frac{dT}{dt} + \frac{dD}{dt} \quad , \tag{1}$$

where U, V, T and D respectively are the work of the external loads, the recoverable internal energy, the kinetic energy, and the sum of all dissipated energies such as surface tension, plastic work, viscous dissipation, etc. If the energy dissipation takes place only around the advancing periphery of the crack, in the quasi-static case T is negligible and defining $dD/dA=\mathcal{G}_c$, (1) may be expressed as

$$\frac{d}{dA}(U-V) = \mathcal{G}_c \quad . \tag{2}$$

In the fracture criterion given by (2) the left hand side is the energy available and $\mathcal{G}_c$ is the energy required to create a unit area of new fracture surface. They are also known as the *crack driving force* and the *fracture toughness*, respectively.

If the solid is brittle or quasi brittle, the characteristic size of the zone of energy dissipation around the crack front is generally small in comparison with the length parameter of the crack. It may, therefore, be assumed that the energy (U-V) flowing into the fracture zone will come from the elastic bulk of the solid and will not be critically dependent on the details of the stress state very near the crack tip. Furthermore, it is also clear that in this case the stress state in the elastic bulk of the actual solid will not differ from a purely elastic solution to any significant extent. Consequently, one may be justified in calculating the crack driving force by using the linear elastic crack solution. By using the concept of crack closure it can then be shown that the increment d(U-V) of the energy available for fracture may be evaluated from the asymptotic stresses and the crack opening displacements near the crack tip which, in turn, may be obtained from the three dimensional elasticity solution as follows:

$$\sigma_{ij}(r,\theta) \cong \frac{k_1}{\sqrt{2r}} f_{1ij}(\theta) + \frac{k_2}{\sqrt{2r}} f_{2ij}(\theta) \ , \ (i,j = x,y) \ , \tag{3}$$

$$\sigma_{iz}(r,\theta) \cong \frac{k_3}{\sqrt{2r}} f_{3i}(\theta) \ , \ (i = x,y) \ , \tag{4}$$

$$v^+ - v^- \cong \frac{2(1-\nu^2)}{E} k_1 \sqrt{2r} \ , \ u^+ - u^- \cong \frac{2(1-\nu^2)}{E} \kappa_2 \sqrt{2r} \ , \tag{5}$$

$$w^+ - w^- \cong \frac{k_3}{\mu} \sqrt{2r} \tag{6}$$

where k_1, k_2 and k_3 are the modes I, II, and III stress intensity factors, f_{1ij}, f_{2ij} and f_{3i} are known functions and E, ν and μ are the elastic constants, $E = 2\mu(1+\nu)$. From the crack closure energy it may then be shown that

$$\mathcal{G}_1 = \frac{\pi(1-\nu^2)}{E} k_1^2 \ , \ \mathcal{G}_2 = \frac{\pi(1-\nu^2)}{E} k_2^2 \ , \ \mathcal{G}_3 = \frac{\pi}{2\mu} k_3^2 \ , \tag{7}$$

$$\mathcal{G} = \frac{d}{dA}(U-V) = \mathcal{G}_1 + \mathcal{G}_2 + \mathcal{G}_3 \tag{8}$$

where $\mathcal{G}$ is the total energy available for fracture.

Equation (7) indicates that one may also use k_i in place of $\mathcal{G}_i$ as the measure of the crack driving force. For mode I loading conditions, for example, defining

$$K_I = k_1\sqrt{\pi} \ , \ \mathcal{G}_{1c} = \mathcal{G}_{IC} \ , \ K_{IC} = \sqrt{\mathcal{G}_{IC}E/(1-\nu^2)} \ , \tag{9}$$

the fracture criterion (2) may be expressed as

$$K_I \le K_{IC} \ . \tag{10}$$

Equation (10) has proved to be very useful in considering the fracture stability. However, perhaps the most useful application of the stress intensity factors may be found in analyzing the subcritical crack growth processes.

3.2 Fracture Mechanics of Graded Materials-Embedded Cracks

In studying the fracture mechanics of FGMs one may have to deal with a number of distinct problem areas. The first is the investigation of the nature of stress singularities near the tip of a crack embedded ina nonhomogeneous medium. The second is the general problem of debonding and the effect of a possible "kink" in material property distributions on the behavior of stress singularities. The third is the basic surface cracking problem and the nature of the stress singularities for cracks intersecting the interfaces. The fourth is the problem of stress relaxation due to periodic surface cracking in FGM coatings. The fifth significant problem area is concerned with the stress concentrations and the resulting delamination cracking at the free ends of FGM coated homogeneous substrates under residual or thermal stresses. In the following sections these problem areas are briefly discussed and some examples are given.

To examine the influence of the material nonhomogeneity on the asymptotic stress state near the crack tips, we first consider the plane elasticity problem for an infinite medium containing a line crack (Fig. 1). For simplicity we will assume that the Poisson's ratio ν of the medium is constant and the shear modulus is approximated by

$$\mu(x,y) = \mu_0 \exp(\beta x + \gamma y) \ , \tag{11}$$

where μ_0, β and γ are known constants. This problem was solved for a crack along y=0, -a<x<a under arbitrary loading conditions [12*], [22*]. It was shown that near the crack tip x=a the stresses have the following asymptotic behavior:

$$\sigma_{ij}(x,y) = \exp[r(\beta\cos\theta + \gamma\sin\theta)]\left[\frac{k_1}{\sqrt{2r}} f_{1ij}(\theta) + \frac{k_2}{\sqrt{2r}} f_{2ij}(\theta)\right], \ (i,j = x,y), \tag{12}$$

where the stress intensity factors k_1 and k_2 are defined by

$$k_1(a) = \lim_{x\to a}\sqrt{2(x-a)}\sigma_{yy}(x,0) \ , \quad k_2(a) = \lim_{x\to a}\sqrt{2(x-a)}\sigma_{xy}(x,0) \ , \tag{13}$$

and the functions f_{1ij} and f_{2ij} are *identical* to those found for the *homogeneous* materials given in (3). Note that the asymptotic stress states for homogeneous materials (3) and FGMs (12) are identical only at r=0. However, since the crack opening displacement is also influenced in a way similar to stresses, the crack driving force (or, for "fixed grip" conditions, the strain energy release rate) was found to be identical to that calculated for the homogeneous materials, namely

$$\mathcal{J} = \frac{\pi(1+\kappa)}{8\mu(a,0)}(k_1^2 + k_2^2) \tag{14}$$

where κ=3-4ν for plane strain and κ=(3-ν)/(1+ν) for plane stress conditions.

Some sample results for an embedded crack of length 2a in an infinite medium under plane strain conditions are given in Table 1. Referring to Fig. 1 and (11) we first define

$$x' = x\cos\theta + y\sin\theta \ , \ \beta = \omega\cos\theta \ , \ \gamma = \omega\sin\theta \ , \ \omega^2 = \beta^2 + \gamma^2 \ , \tag{15}$$

$$\mu(x,y) = \mu(x') = \mu_0\exp(\omega x') \ . \tag{16}$$

The medium is assumed to be loaded by fixed grips away from the crack region with $\varepsilon_{y'y'}(x',\mp\infty) = \varepsilon_0$. Thus, the normalizing stress intensity factor for the results given in the table is

$$k_0 = 2(1+\nu)\mu_0\varepsilon_0\sqrt{a} \ . \tag{17}$$

Note that the crack orientation angle θ=0 corresponds to a mode I problem for which $k_2(\mp a) = 0$, whereas for $\theta = \pi/2$ the loading is parallel to the crack and, consequently,

Table 1. The effect of material nonhomogeneity parameter $a\omega$ and the crack orientation angle θ on the stress intensity factors; ν=0.3; loading: uniform strain away from the crack region, $\varepsilon_{y'y'}(x', \mp\infty) = \varepsilon_0$.

$a\omega$	θ/π	$k_1(a)/k_0$	$k_1(-a)/k_0$	$k_2(a)/k_0$	$k_2(-a)/k_0$
	0	1.196	0.825	0	0
	0.1	1.081	0.750	-0.321	-0.254
	0.2	0.781	0.548	-0.514	-0.422
0.25	0.3	0.414	0.290	-0.504	-0.437
	0.4	0.121	0.075	-0.304	-0.282
	0.5	0	0	0	0
	0	1.424	0.674	0	0
	0.1	1.285	0.617	-0.344	-0.213
	0.2	0.925	0.460	-0.548	-0.365
0.5	0.3	0.490	0.247	-0.532	-0.397
	0.4	0.146	0.059	-0.314	-0.269
	0.5	0	0	0	0
	0	6.317	0.115	0	0
	0.1	5.376	0.117	-0.867	-0.037
	0.2	3.315	0.115	-1.155	-0.090
2.5	0.3	1.441	0.082	-0.900	-0.158
	0.4	0.369	0.004	-0.429	-0.179
	0.5	0	0	0	0

Table 2. Stress intensity factors for a plane strain and a penny-shaped crack in a graded medium under tension σ_0 perpendicular to the plane of the crack; ν=0.3.

ωa	0	0.1	0.25	0.5	1.0	2.5	5.0
Plane Strain Crack							
$k_1/\sigma_0\sqrt{a}$	1	1.008	0.036	1.101	1.258	1.808	2.869
$k_2/\sigma_0\sqrt{a}$	0	0.026	0.065	0.129	0.263	0.697	1.567
Penny-Shaped Crack							
$k_1/\left(\frac{2}{\pi}\sigma_0\sqrt{a}\right)$	1	1.002	1.012	1.038	1.118	1.442	2.083
$k_2/\left(\frac{2}{\pi}\sigma_0\sqrt{a}\right)$	0	0.017	0.041	0.083	0.168	0.440	0.960

all stress intensity factors are zero.

Table 2 shows some limited results comparing plane strain and penny-shaped crack solutions for a graded material under uniform tension σ_0 perpendicular to the plane of the crack where $\omega=0$ corresponds to the results for a homogeneous medium. The table shows that the stress intensity factors in FGMs are higher than that in homogeneous materials and that the influence of the material nonhomogeneity on the stress intensity factors is more severe for a plane strain than for a penny-shaped crack. For further results see [12], [22], [23] and [24]. Also, for the solution of embedded crack problems in an FGM layer under mechanical or thermal loading see [15*] and [16*].

3.3 The Debonding Problems for FGMs

Consider the crack problems shown in Figs. 2a and 2b. Figure 2a describes the debonding problem in piecewise homogeneous materials, whereas Fig. 2b refers to a FGM bonded to a homogeneous substrate. In both cases h=0 refers to an "interface crack". In terms of the unknown functions

$$f_1(x)=\frac{\partial}{\partial x}(v^+-v^-)\ ,\ f_2(x)=\frac{\partial}{\partial x}(u^+-u^-)\ , \tag{18}$$

in each case the formulation of the problem may be reduced to a system of integral equations of the form

$$\frac{1}{\pi}\int_{-a}^{a}\sum_{1}^{2}[\frac{\delta_{ij}}{t-x}+k_{ij}^{s}(x,t)+k_{ij}^{f}(x,t)]f_j(t)dt=\frac{1+\kappa}{2\mu_1(0)}p_i(x)$$

$$(i=1,2)\ ,\ -a<x<a \tag{19}$$

where the kernels k_{ij} are known functions which depend on h and the material parameters, k_{ij}^{s} is associated with the infinite medium, k_{ij}^{f} represents the geometry of the medium, and

$$p_1(x)=\sigma_{yy}(x,0)\ ,\ p_2(x)=\sigma_{xy}(x,0) \tag{20}$$

are the crack surface tractions which may be expressed in terms of the external load. The kernels k_{ij}^{f} are bounded for all values of h. For h>0 the functions k_{ij}^{s} are also bounded. Thus, for h>0 the crack is an embedded crack and (19) would lead to the asymptotic stresses given by (3) and (12) for problems described by Figs. 2a and 2b, respectively.

On the other hand, for h=0 in problem 2a the kernels k_{11}^s and k_{22}^s would become a Cauchy kernel $(t-x)^{-1}$ and k_{12}^s and k_{21}^s would degenerate to a delta function $\delta(t-x)$ [25], [26]. Consequently, in this interface crack problem the integral equations become one of the second kind leading to the well-known anomalous stress oscillation behavior very near the crack tips.

For h=0 in problem 2b, however, the leading terms of the kernels k_{ij}^s become

$$k_{11}^s = k_{22}^s = -\frac{\pi\gamma}{8}\frac{|t-x|}{t-x} \ ,$$

$$k_{12}^s = -k_{21}^s == +\frac{\gamma}{4}\log|t-x| \ , \ \gamma = \tan\phi_0 \ , \tag{21}$$

which would indicate that (19) would remain to be an ordinary system of singular integral equations of the first kind and would have the asymptotic solution given by (12). It is, therefore, seen that the anomalous behavior of the crack tip stress oscillations may be eliminated by "smoothing" the material property distribution (or by removing the property discontinuity). A qualitative description of the interface crack geometries and the singular kernels k_{ij}^s may be seen in Fig. 3.

Figure 4 describes an interface crack problem for a FGM coating bonded to a homogeneous substrate. In actual applications the medium contains an additional layer of bond coat between the substrate and the FGM coating. Typically the materials for the bond coat and the substrate are NiCrAlY and MCrAlY, respectively, wehre M stands for a "metal" (e.g., NiCo). Since in most cases these two materials have approximately the same thermomechanical constants, in the example considered the bond coat is assumed to be an extension of the substrate. Because of the oxide scales (usually Al_2O_3) forming along bond coat/FGM interface, it is also assumed that this interface is the weak cleavage plane and contains a crack of length 2a. In the example h_1 and h_2 are the thicknesses and μ_1 and $\mu_2(y)$ are the shear moduli of the substrate and the FGM, respectively. The nonhomogeneity constant γ is defined by

$$\mu_2(y) = \mu_1 \exp(\gamma y) \ , \ \gamma = \frac{1}{h_2}\log[\mu_2(h_2)/\mu_1] \ . \tag{22}$$

The problem is solved under uniform crack surface pressure, $\sigma_{yy}(x,0) = -\sigma_0$ or shear, $\sigma_{xy}(x,0) = -\tau_0$. In each case the calculated stress intensity factors k_1, k_2 and the strain energy release rate $\mathcal{H}$ are normalized with respect to the following:

$$k_0 = \sigma_0\sqrt{a}\ ,\ k_0 = \tau_0\sqrt{a}\ ,\ \mathcal{H}_0 = \frac{\pi(\kappa+1)}{8\mu_1}\sigma_0^2 a\ ,\ \mathcal{H}_0 = \frac{\pi(\kappa+1)}{8\mu_1}\tau_0^2 a\ , \qquad (23)$$

which correspond to the values obtained for an infinite medium under plane strain conditions and uniform tractions $\sigma_{yy}(x,\mp\infty) = \sigma_0$ or $\sigma_{xy}(x,\mp\infty) = \tau_0$.

Some sample results showing the effect of material nonhomogeneity constant γ and the relative dimensions h_1/a and h_2/a are given in Figures 5-10. In all cases γ=0 corresponds to the homogeneous medium. As physically expected, as γ increases, the stiffness of the coating increases, leading to decreasing crack driving force $\mathcal{H}$.

Clearly the problem is one of mixed-mode and unless the plane of the crack is a weak cleavage plane (e.g., due to oxidation), the crack may not grow in a co-planar fashion. In this case, the stress intensity factors k_1 and k_2 may be used to determine the probable crack growth angle, θ_0. This angle, measured from the positive x axis may be calculated from $\partial\sigma_{\theta\theta}/\partial\theta = 0$, $\sigma_{\theta\theta}(r,\theta_0) > 0$ [27], or

$$k_1\sin\theta_0 + k_2(3\cos\theta_0 - 1) = 0\ ,$$

$$k_1\cos^2\frac{\theta_0}{2} - \frac{3}{2}k_2\sin\theta_0 > 0\ . \qquad (24)$$

Some calculated values of θ_0 for ν=0.3, h_1/a=100, h_2/a=0.25, 0.5, 1, 2, 10 and for uniform crack surface presure σ_0 are shown in Fig. 11. The figure indicates that if the medium is isotropic with regard to the crack growth resistance $\mathcal{H}_c$ near the crack tip, maximum strain energy release and, as a result, further crack growth would take place in a direction toward the less stiff material. On the other hand, if $\mathcal{H}_c$ is θ-dependent, then the crack growth direction θ_0 would be determined by maximizing $\mathcal{H}(\theta)/\mathcal{H}_c(\theta)$, $\mathcal{H}(\theta)$ being the strain energy release rate for a small radial crack extension in the direction of θ. Further results may be found in [14*].

It should be noted that in formulating this problem the crack surface tractions are assumed to be arbitrary functions of x. Therefore, the technique described in [14*] may

be used to solve any quasi-static interface crack problem involving FGM coatings after properly separating the solution for the uncracked problem. Also, for the validity of the solution it is essential that the normal crack opening v^+-v^- be positive. Otherwise the problem must be treated as a crack/contact problem, the condition $k_I(-a)$ determining the crack closure point [16*].

3.4 Cracking perpendicular to interfaces and surfaces

In ceramic and ceramic/metal FGM components generally a common mode of failure is surface cracking which could penetrate to the interface and cause spallation. The main problem here is assessing the influence of the material nonhomogeneity on the fracture mechanics parameters (such as $\mathcal{b}$ and k_1) for surface cracks and cracks terminating at an interface. Figures 2c and 2d show the crack geometry for the latter problem in piecewise homogeneous and in nonhomogeneous materials. Because of symmetry, generally these are all mode I problems. Thus, if we define the unknown function and the crack surface traction by

$$g(x) = \frac{\partial}{\partial x}[v(x,+0) - v(x,-0)] \ , \ p(x) = \sigma_{yy}(x,0) \ , \ a < x < b \ , \tag{25}$$

the integral equation for the general problem may be expressed as

$$\frac{1}{\pi}\int_a^b [\frac{1}{t-x} + k_s(x,t) + k_f(x,t)]g(t)dt = \frac{1+\kappa_2}{2\mu_2} p(x) \ , \ a < x < b \ , \tag{26}$$

where, again, k_s is associated with two bonded semi-infinite media, k_f represents the geometry of the composite medium, and k_f is always bounded. for an embedded crack, a>0 and k_s is also bounded. However, for a=0, k_s could be singular. In fact, for a=0 in piecewise homogeneous materials (Fig. 2c) it is known that

$$k_s(x,t) = \frac{c_1}{t+x} + \frac{c_2 x}{(t+x)^2} + \frac{c_3 x^2}{(t+x)^3} \ , \ (0 < (t,x) < b) \ , \tag{27}$$

where c_1, c_2, and c_3 are bimaterial constants [28]. Note that as t and x approach the end point x=0, k_s tends to infinity and, hence, would contribute to the singular behavior of the solution giving

$$\sigma_{ij}(r,\theta) = \frac{k_1}{r^{\alpha}} g_{ij}(\theta) \ , \ 0 \le \theta \le \pi \ , \ (i,j = x,y) \ , \ 0 < \alpha < 1 \qquad (28)$$

where g_{ij} are known functions, k_1 is a "stress intensity factor" and the power of stress singularity α is a function of the bimaterial constants. Generally $\alpha>1/2$ for $\mu_2>\mu_1$ and $\alpha<1/2$ for $\mu_2<\mu_1$, $\alpha=1/2$ being the value for $\mu_2<\mu_1$. From the viewpoint of fracture mechanics, the consequence of having $\alpha\neq1/2$ is that as the crack intersects the interface, the stress and deformation states would not remain self-similar and, hence, it would not be possible to use the fracture theories based on the energy balance concept to calculate a strain energy release rate or to use the stress intensity factors as the crack driving force. This, then, is the second anomalous behavior regarding the stress state near the crack tip in bonded dissimilar homogeneous materials.

If we now "smooth" the material property distribution and assume that medium 1 is a FGM (Fig. 2d), it can be shown that for a=0 the leading terms of k_s become [29]

$$k_s(x,t) \cong \frac{d_1 t}{t+x} + \frac{d_2 x}{t+x} + \frac{d_3 t x}{(t+x)^2} + d_4 \log(t+x) \qquad (29)$$

where $d_1 ... d_4$ are bimaterial constants. Note that the kernel given by (29) is square integrable and, therefore, would have no contribution to the stress singularity at x=0. Consequently, the stresses would have the standard square-root singularity and, by smoothing the material property distribution through the introduction of FGM, the anomalous behavior of the stress state would again be eliminated.

Figure 12 shows the mode I stress intensity factor for a=0 and $p(x)=-\sigma_0$ in Fig. 2d. The normalized stress intensity factors shown in the figure are defined by

$$k(a) = k_1(0)/\sigma_0\sqrt{b/2} \ , \ k(b) = k_1(b)/\sigma_0\sqrt{b/2} \ , \qquad (30)$$

$$k_1(0) = \lim_{x\to 0}\sqrt{-2x}\sigma_{1yy}(x,0) \ , \ k_1(b) = \lim_{x\to b}\sqrt{2(x-b)}\sigma_{2yy}(x,0) \ . \qquad (31)$$

The shear modulus of FGM in Fig. 2d is assumed to be

$$\mu_1(x) = \mu_2 \exp(\beta x) \qquad (32)$$

where μ_2 is constant. It is thus seen that for $\beta\to\infty$ $\mu_1\to0$ and the problem becomes an ordinary edge crack problem in a homogeneous half space for which

$$k_1(0) \to \infty \ , \ k_1(b) \to 1.5861\,\sigma_0\sqrt{b/2} \ . \qquad (33)$$

For $\beta=0$ the medium is homogeneous and

$$k_1(0) = k_1(b) = \sigma_0\sqrt{b/2} \quad . \tag{34}$$

In the other limiting case of $\beta=-\infty$, μ_1 becomes infinite and for the resulting problem of a crack terminating at the interface we have

$$k_1(0) \to 0 \ , \ k_1(b) \to 0.8710\ \sigma_0\sqrt{b/2} \quad . \tag{35}$$

The analytical details and further results for this problem may be found in [29].

The basic problem of surface cracking in a FGM layer is shown in Fig. 13. In this case equations (25) defining the unknown and input functions and (26) describing the form of the integral equation are still valid. In the surface crack problem under consideration it can be shown that [15*]

$$k_s(x,t) = -\frac{1}{t+x} + \frac{6x}{(t+x)^2} - \frac{4x^2}{(t+x)^3} \quad , \tag{36}$$

which is identical to the singular kernel found for a homogeneous medium with an edge crack [28].

Some sample results for the layer shown in Fig. 13 under fixed-grip loading or constant strain $\varepsilon_{yy}^{\infty} = \varepsilon_0$, membrane loading N and bending moment M are given in Figures 14-19. Figures 14-16 show the stress component σ_{yy} in the uncracked layer. In this problem, too, it is assumed that the Poisson's ratio is constant and the Young's modulus at x=0 and x=h is given by E_1 and E_2, respectively, E_2/E_1 being the measure of material nonhomogeneity. The Young's modulus E(x) and the material nonhomogeneity parameter γ are defined by

$$E(x) = E_1 e^{\gamma x} \ , \ \gamma = \frac{1}{h}\log(E_2/E_1) \ . \tag{37}$$

The normalizing stresses shown in the figures are defined by

$$\sigma_0 = E_1\varepsilon_0/(1-\nu^2) \ , \ \sigma_t = N/h \ , \ \sigma_b = 6M/h^2 \quad . \tag{38}$$

Note that the results given for E_2/E_1=1, 2, 5, 10, 20 in Figures 15 and 16 may also be interpreted for E_2/E_1=1, 0.5, 0.2, 0.1, 0.05, respectively. The membrane resultant N_{yy}=N is applied along x=h/2 away from the crack region. Since the ends are free to rotate the stress distribution shown in Fig. 15 exhibits considerable bending effect.

The mode I stress intensity factors k_1 corresponding to the stresses shown in Figures 14-16 are given in Figures 17-19, respectively. In Figure 17, the normalizing stress σ_0 is the value of σ_{yy} at x=0 in the uncracked medium. Thus, for all values of E_2/E_1, as the crack length b approaches zero, $k_1/\sigma_0\sqrt{b}$ would approach 1.1215, the edge crack solution for a homogeneous half plane [28]. Similarly, note that under membrane loading and bending, as b→0, the limiting value of the stress intensity factor would tend to

$$k_1(b) = 1.1215\,\sigma_{yy}(0)\sqrt{b}\ , \quad (b << h) \tag{38}$$

where $\sigma_{yy}(x)$ is the stress in the uncracked medium. It should be observed that in all cases $k_1(b)$ becomes unbounded as b→h (Figures 17-19).

Some results for a surface crack in a FGM layer under thermal loading are shown in Figures 20-23. Figure 20 shows the stress distribution $\sigma_{yy}(x)$ in a FGM layer with $E_2/E_1=5$ and $\alpha_2/\alpha_1=2$ undergoing a uniform temperature change $T-T_0$, where α is the thermal expansion coefficient. Note that the temperature is normalized with respect to T_0 and $(T-T_0)/T_0=(T/T_0)-1$. Hence, the stress $\sigma_{yy}(x)$ is lienarly dependent on $(T/T_0)-1$. In all cases the normalizing stress is defined by

$$\sigma_0 = E_1\alpha_1 T_0/(1-\nu)\ . \tag{39}$$

The stress $\sigma_{yy}(x)$ for a steady-state heat conduction problem in a FGM layer with $E_2/E_1=10$, $\alpha_2/\alpha_1=2$ and $\lambda_2/\lambda_1=10$ is shown in Fig. 21, where $\lambda(x)$ is the coefficient of heat conduction. In these examples the functions E(x), $\alpha(x)$ and $\lambda(x)$ are assumed to be of the form given by (37). The normalized stress intensity factors for an edge crack in a FGM layer (Fig. 13) under thermally induced stresses given by Figures 20 and 21 are shown in Figures 22 and 23, respectively. In these figures the normalizing stress intensity factor is $\sigma_0\sqrt{b}$ where σ_0 is defined by (39).

The analytical details of the solution of the surface crack problems and further results may be found in [15*] and [16*].

3.5 Stress Relaxation Due to Periodic Surface Cracking

The mud-flat type periodic surface cracking of ceramics or ceramic coatings under residual or thermal stresses seems to be a commonly observed mechanism through which the stresses or energy are relieved. Usually such materials are under in-plane biaxial strains of equal magnitude. An important mechanics problem here is the determination of the length parameter describing the surface crack periodicity in terms of the biaxial strain ε_0 and the fracture touchness $\mathcal{b}_c$. A highly simplified technique used in practice largely for screening purposes is an energy balance approach [30]. It is usually assumed that in a single "cell" formed by surface cracks, the energy available for fracture is provided by the strain energy within the cell, whereas the energy needed to create the fracture surfaces is the energy sink. The major assumption here is that, as a result of cracking, the entire strain energy inside the volume of the cell is released, which, in piecewise homogeneous materials, leads to the following energy balance relation:

$$U_R = U_D \ , \ \mathrm{U_R} = AbW \ , \ U_D = Sb(\mathcal{b}_c / 2) \ , \ W = \varepsilon_0^2 E / (1-\nu) \ , \qquad (40)$$

where U_R is the strain energy per cell, U_D is the dissipated energy per cell, A is the surface area of the cell, b is the crack depth, W is the strain energy density, S is the peripheral length of the crack for a single cell, and $\mathcal{b}_c/2$ is the energy required to create a unit fracture surface. If the cell is an n-sided regular polygon with center to apex distance c, then

$$A = \frac{n}{2} c^2 \sin(\frac{2\pi}{n}) \ , \ S = 2nc \ \sin(\frac{\pi}{n}) \ . \qquad (41)$$

The shape of the polygon or n must be such that for a unit surface area U_R/U_D is maximum. For the purpose of determining n one may assume that A is "unity". Thus, eliminating c, for given ε_0 and $\mathcal{b}_c/2$ the condition U_R/U_D=max. may be replaced by A/S=max., from which it would follow that

$$(A / S) = \frac{1}{2}(n \ \tan(\frac{\pi}{n}))^{-1/2} = \text{max.} \qquad (42)$$

Technically, (42) gives the expected result, namely n=∞ or a circular cell. However, since the plane cannot be divided continuously into circles of equal radii, physically this result is not acceptable. The admissible regular polygons are triangle, square and

hexagon. Since A/S is a monotonously increasing function of n, the acceptable solution of (42) would be n=6 or a regular hexagon, which is generally the observed result [30].

For hexagonal cells we have $A = 3\sqrt{3}c^2/2$, S=6c and from (40) we find

$$c\varepsilon_0^2 = \frac{2(1-\nu)}{\sqrt{3}E}\,\mathcal{b}_c \tag{43}$$

where c is the length of the side of the hexagon. Equation (43) gives the relationship between the cell size and the biaxial strain in the general periodic surface cracking problem. Note that in this simple model the criterion found is independent of the crack depth.

Similar results may be obtained if we assume the cracking medium (constrained single layer or coating) is FGM. For hexagonal surface cracking from the energy balance equation $U_R=U_D$ it may easily be shown that

$$c\varepsilon_0^2 = \frac{2}{\sqrt{3}}\left(\int_0^b \mathcal{b}_c(x)dx\right) / \left(\int_0^b E(x)dx/(1-\nu)\right) \tag{44}$$

where $\mathcal{b}_c$ and E are the fracture toughness and Young's modulus of FGM and b is the crack depth. Note that in FGMs the cell size vs. biaxial strain relationship found is now dependent on the crack depth. It is possible that (44) may again be useful for screening purposes if one assumes the crack depth to be equal to a certain percentage of the FGM coating thickness h.

The preceding technique is very highly approximate. Since the corresponding three-dimensional elasticity problem for the periodic surface cracks is analytically intractable, to shed some light on the subject one may consider a simple two-dimensional problem. The simplest such problem of periodic surface cracking of a FGM coating bonded to a homogeneous substrate under antiplane shear loading was recently considered in [17*]. In this study it was assumed that the substrate is a half space having the shear modulus μ_2 and the shear modulus of the FGM is given by

$$\mu_1(x) = \mu_1(0)\exp(\beta x)\ ,\ \beta = \frac{1}{h}\log\left(\frac{\mu_2}{\mu_1(0)}\right) \tag{45}$$

where $\mu_1(0)$ is the shear modulus of FGM on the surface, x=0, and h is the thickness of the coating. It is further assumed that the coating contains periodic surface cracks with the period 2c and depth b, and the medium is subjected to a constant strain $2\varepsilon_{yz}(x,\mp\infty)=\gamma_0$ through fixed grips (Fig. 24).

The results of an example showing the stress relaxation on the surface of the coating as a result of periodic cracking are shown in Figures 25 and 26. Note that as c/h→0 the surface stress $\sigma_{1yz}(0,y)$ would tend to zero everywhere and, as c/h→∞, $\sigma_{1yz}(0,c)$ would approach τ_0, the surface shear stress for the uncracked coating. We also note that the previous simple periodic cracking model assumes the stress to be zero within the entire cell, that is, $\sigma_{1yz}(0,y)=0$, $0<y<c$. Figures 25 and 26 show that this is hardly the case.

Another interesting result of this study is shown in Figures 27 and 28. Here V_1 is the actual strain energy released per unit area of the coating as a result of periodic cracking. V_1 is calculated from the elasticity solution for the cracked medium. U_1 is the total strain energy contained in the volume 1x1xb and is calculated from

$$U_1 = U_R / 2c \ , \ U_R = c\gamma_0^2 \int_0^b \mu(x)dx \ . \tag{46}$$

Clearly, the physics of the problem requires that

$$\lim_{c\to 0} V_1 = U_1 \ . \tag{47}$$

Figures 27 and 28 show that the assumption made for the previous simple model to the effect that the entire strain energy contained within the cell is relieved and is transformed into fracture energy may be justified only for very small values of c/h and, in general, only a certain percentage of the total energy is available to overcome the fracture energy.

Figures 29 and 30 show the way one may use the basic results giving the stress intensity factor as a function of the crack depth in fracture stability studies in FGM coatings. Assuming that near the surface the FGM is 100% ceramic and near the interface 100% metal, in this example the mode III fracture resistance parameter k_{3c} obtained from

$$k_{3c}(x) = [2\mu(x)\delta_{3c}(x)/\pi]^{1/2} \tag{48}$$

is taken to be an increasing function of x as shown in the figures. Consequently, the FGM coating would exhibit an R-curve (crack-extension-resistance-curve) behavior. That is, since the fracture toughness increases with increasing crack length, the load amplitude must be increased continuously to keep the crack growing. Thus, the threshold value $\tau_T = \mu_1(0)\gamma_{0T}$ and the critical value $\tau_c = \mu_1(0)\gamma_{0c}$ may be obtained by requiring that the corresponding $k_3(b)$ curves envelope $k_{3c}(x)$ from below and from above, respectively. For $\tau_T < \tau_0 < \tau_c$ the crack would grow in an unstable manner in the region for which $k_3 > k_{3c}$ and becomes arrested when $k_3 \leq k_{3c}$.

Extensive results on the periodic cracking of FGM coatings under Mode III loading conditions may be found in [17*]. The plane strain problem of periodic cracking for a homogeneous coating and for a single homogeneous layer subjected to membrane loading or bending was considered in [18*].

3.6 End Effects on Stress Concentration and Edge Debonding

Generally the stress-free ends in bonded materials are locations of high stress concentrations and potential debonding fracture. In bonded dissimilar homogeneous materials the point at which the interface intersects the free boundary (or the apex of two 90 degree bonded wedges) is, in fact, a point of singularity near which the stress state is given by [31]

$$\sigma_{ij}(r,\theta) = \frac{K}{r^{\beta}} F_{ij}(\theta) \ , \ (i,j = x,y) \ , \ 0 < \beta < 1/2 \ , \tag{49}$$

when (r,θ) are the polar coordinates, β and F_{ij} depend on the bimaterial constants and K is a measure of the load amplitude or stress intensity. For β to be positive the material properties need to be discontinuous across the interface. In FGM coatings, since the material properties are made continuous through composition grading, it can be shown that the singularity β becomes zero and, consequently, the stresses become finite [32].

Figure 31 describes the geometry of a specimen considered as an example. The composite medium is assumed to undergo a homogeneous temperature change ΔT. The problem is one of plane strain. The substrate is a nickel-based superalloy (Rene 41) and the coating is either a piecewise homogeneous or a functionally graded metal/ceramic

layer, the ceramic component being partially stabilized zirconia (PSZ). The thermomechanical constants of the two materials are

E_s=219.7 GPa , ν_s=0.3 , α_s=1.67x10^{-5}°K^{-1} ,

E_c=151 GPa , ν_s=0.3 , α_c=10^{-5}°K

where the subscripts s and c refer to the substrate and the ceramic, respectively. The stepwise variation of the material properties in piecewise homogeneous coatings is shown in Fig. 32. Some calculated results are shown in Figures 33-37. For the FGM coating used in the example, the modulus variation is given by

$$E(y) = \begin{cases} E_s , & 0<y<0.0125 \text{ m.} \\ E_c+(E_s-E_c)\left(\dfrac{0.0145-y}{0.002}\right)^p , & 0.0125<y<0.0145 \text{ m.} \end{cases}$$

The same expression is ued for the thermal expansion coefficient, α. Figure 38 shows the thickness variation of the stiffness E(y) (or the thermal expansion coefficient α(y) for the three FGMs considered, namely the metal-rich, linear and ceramic rich compositions.

Figures 33 and 34 show the interface stresses $\sigma_{yy}(x,h_2)$ and $\sigma_{xy}(x,h_2)$ for the piecewise homogeneous coating. Note that since the material properties are discontinuous for $y=h_2$, the interface stresses become unbounded for $y=h_2$, $x\rightarrow\ell$. The corresponding results for the FGM coatings are shown in Figures 35 and 36. It may be observed that as a result of material property smoothing (or eliminating the property discontinuities), the stress singularities are eliminated and at the point $y=h_2$, $x=\ell$ $\sigma_{yy}(x,h_2)$ becomes bounded and $\sigma_{xy}(x,h_2)$ becomes zero. One may also observe that, except for values of x near the end ($x=\ell$), the behavior of interface stresses for piecewise homogeneous and FGM coatings are quite similar. Figure 37 shows the variation of the tensile stress $\sigma_{yy}(\ell,y)$ at the ends of the specimen for $0<y<h_1+h_2$. Note that at the interface $y=h_2$ there is a stress concentration and the stress concentration factor σ_{yy}/σ_0 decreases with increasing metal content of the coating. Further results on this problem may be found in [8*].

The effect of material orthotropy on the crack driving force for homogeneous debonding layers was considered in [19*] and [20*]. In [19*] the plane strain problem of

debonding crack initiating from a free end was studied. The problem of a T-shaped crack simulating the debonding process that is initiated from a surface crack terminating at the coating/substrate interface was considered in [20*].

3.7 Some Concluding Remarks

From the viewpoint of fracture mechanics the "functionally graded materials" seem to offer certain advantages among which one may mention the following:

(i) By eliminating the discontinuity in material property distributions, the mathematical anomalies regarding the crack tip stress oscillations for the interface cracks and the non-square-root singularities for the cracks intersecting the interfaces are also eliminated. In practice the importance of this result lies in the fact that in FGMs one can now use the crack tip finite element modeling developed for the ordinary square-root singularity and apply the methods of the energy balance-based theories of the conventional fracture mechanics.

(ii) Application of FGMs as interfacial zones in joining generally incompatible materials would greatly improve the bonding strength.

(iii) Use of FGMs as coatings and interfacial zones would reduce the magnitude of the residual and thermal stresses.

(iv) Use of FGM coatings and interfaces would eliminate the stress singularities at the points of intersection of interfaces and stress-free ends in bonded materials.

(v) Replacing homogeneous coatings by FGM layers would both enhance the bonding strength and reduce the crack driving force.

4. REFERENCES(*)

1. T. Hirano, T. Yamada, J. Teraki, M. Niino and A. Kumakawa, Proc. 16th Int. Symp. on Space Technology and Science, Sapporo, Japan, May 1988.

(*) Research reported in References marked by an (*) was fully or partly supported by the AFOSR Grant.

2. M. Yamanouchi, M. Koizumi, T. Hirai and I. Shiota, eds. FGM-90, Proc. of the First Int. Symp. on Functionally Gradient Materials, FGM Forum, Sendai, Japan, 1990.

3. K. Muramatsu, A. Kawasaki, M. Taya and R. Watanabe, FGM-90, p. 53, FGM Forum, Sendai, Japan, 1990.

4. A. Kawasaki and R. Watanabe, FGM-90, p. 197, FGM Forum, Sendai, Japan, 1990.

5. J.B. Holt, M. Koizumi, T. Hirai and Z.A. Munir, eds., Proc. of the Second Int. Symp. on Functionally Gradient Materials, Ceramic Transactions, Vol. 34, American Ceramic Society, Westerville, OH, 1993.

6. B. Ilschner and N. Cherradi, eds., Proc. of the Third Int. Symp. on Structural and Functional Gradient Materials, Presses Polytechniques et Universitaires Romands, Lausanne, Switzerland, 1995.

7. S. Sampath, H. Herman, N. Shimoda and T. Saito, MRS Bulletin, p. 27, January 1995.

8.* Y-D. Lee and F. Erdogan, "Residual/Thermal Stresses in FGM and Laminated Thermal Barrier coatings," AFOSR Project Report, 1994. (Also published in *Int. J. of Fracture*, Vol. 69, pp. 145-165, 1995).

9. B.H. Rabin and I. Shiota, MRS Bulletin, p. 14, January 1995.

10. K. Kurihara, K. Sasaki and M. Kawarada, FGM-90, p. 65, FGM Forum, Sendai, Japan, 1990.

11. W.Y. Lee, Y.W. Bae, C.C. Berndt, F. Erdogan, Y.D. Lee and Z. Mustasim, Advanced Turbine Systems - Materials Workshop, Charleston, SC, Feb. 13-14, 1996 (submitted for publication, J. Amer. Cer. Soc., 1996).

12.* F. Erdogan, "Fracture Problems in Functionally Gradient Materials," AFOSR Project Report, 1994. (Also published in *Tr. Journal of Engineering and Environmental Sciences*, Vol. 5, pp. 753-770, 1995).

13.* M. Ozturk and F. Erdogan, "Axisymmetric Crack Problem in Bonded Materials with a Graded Interfacial Region," AFOSR Project Report, 1994. (Also published in *Int. J. Solids Structures*, Vol. 33, pp. 193-217, 1996).

14.* Y-F. Chen and F. Erdogan, "The Interface Crack Problem for a Nonhomogeneous Coating Bonded to a Homogeneous Substrate," AFOSR Project Report, 1995. (Also published in *J. Mech. Phys. Solids*, Vol. 44, pp. 771-787, 1996).

15.* F. Erdogan and B-H. Wu, "The Surface Crack Problem for a Plate with Functionally Graded Properties," AFOSR Project Report, 1994. (Also submitted for publication to the *ASME J. Appl. Mech.*).

16.* F. Erdogan and B-H. Wu, "Crack Problems in FGM Layers under Thermal Stresses," AFOSR Project Report, 1995. (Also to be published in *Journal of Thermal Stresses*, 1996).

17.* F. Erdogan and M. Ozturk, "Periodic Cracking of Functionally Graded Coatings." AFOSR Project Report, 1994. (Also published in *Int. J. of Engng. Sci.*, Vol. 33, pp. 2179-2195, 1995).

18.* G.W. Schulze and F. Erdogan, "Periodic Cracking of Elastic Coatings," AFOSR Project Report, 1995. (Also submitted for publication to *Int. J. Solids Structures*, 1996).

19.* S. Kadioglu and F. Erdogan, "Edge Debonding in Layered Materials", AFOSR Project Report, 1994. (A modified version, "The Free-End Interface Crack Problems for Bonded Orthotropic Layers," has ben published in *Int. J. Engng. Sci.*, Vol. 33, pp. 1105-1120, 1995.)

20.* F. Erdogan and S. Kadioglu, "Stress Intensity Factors for a T-Shaped Crack in Layered Materials," AFOSR Project Report, 1994. (A modified version, "T-Shaped Crack Problem for Bonded Orthotropic Layers," has been published in *Int. J. of Fracture*, Vol. 67, pp. 273-300, 1994.)

21.* F. Erdogan, "Fracture Mechanics of Functionally Graded Materials," Composites Engineering, Vol. 5, pp. 753-770, 1995.

22. N. Konda and F. Erdogan, *Engineering Fracture Mechanics*, Vol. 47, pp. 533-545, 1994.

23. F. Delale and F. Erdogan, *ASME Journal of Applied Mechanics*, Vol. 50, pp. 609-614, 1983.

24. M. Ozturk and F. Erdogan, *ASME Journal of Applied Mechanics*, Vol. 60, pp. 406-413, 1993.

25. F. Erdogan and G.D. Gupta, *Int. J. Solids Structures*, Vol. 7, pp. 39-61, 1971.

26. F. Erdogan and G.D. Gupta, *Int. J. Solids Structures*, Vol. 7, pp. 1089-1107, 1971.

27. F. Erdogan and G.C. Sih, *J. Basic Engng.*, Trans. ASME, Vol. 85, pp. 519-525, 1963.

28. T.S. Cook and F. Erdogan, *Int. J. Engng. Sci.*, Vol. 10, pp. 667-696, 1972.

29. F. Erdogan, A.C. Kaya and P.F. Joseph, *ASME Journal of Applied Mechanics*, Vol. 58, pp. 40-418, 1991.

30. H.A. Nied, "Criterion for Predicting Segmentation Cracking on Surfaces of Brittle Materials," GE/CRD Report 90CRD258, 1990.

31. F. Erdogan and V. Biricikoglu, *Int. J. Engng. Sci.*, Vol. 11, pp. 645-766, 1973.

32. M. Kasmalkar, Ph.D. Dissertation, Lehigh University, 1996.

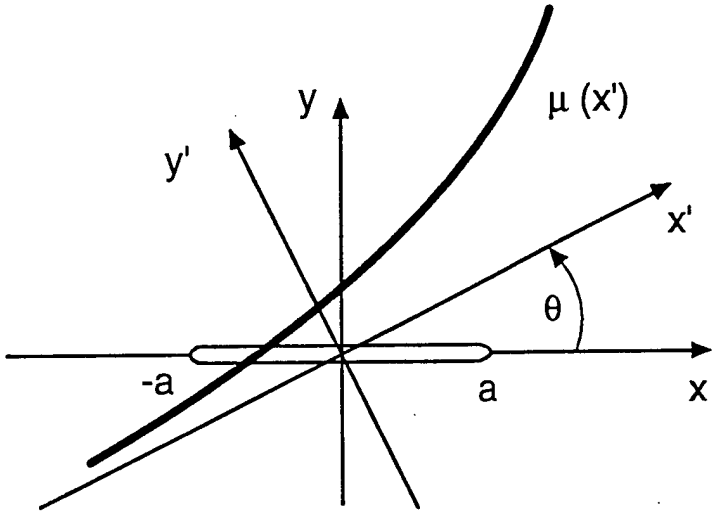

Figure 1: Notation for a plane crack in a nonhomogeneous medium.

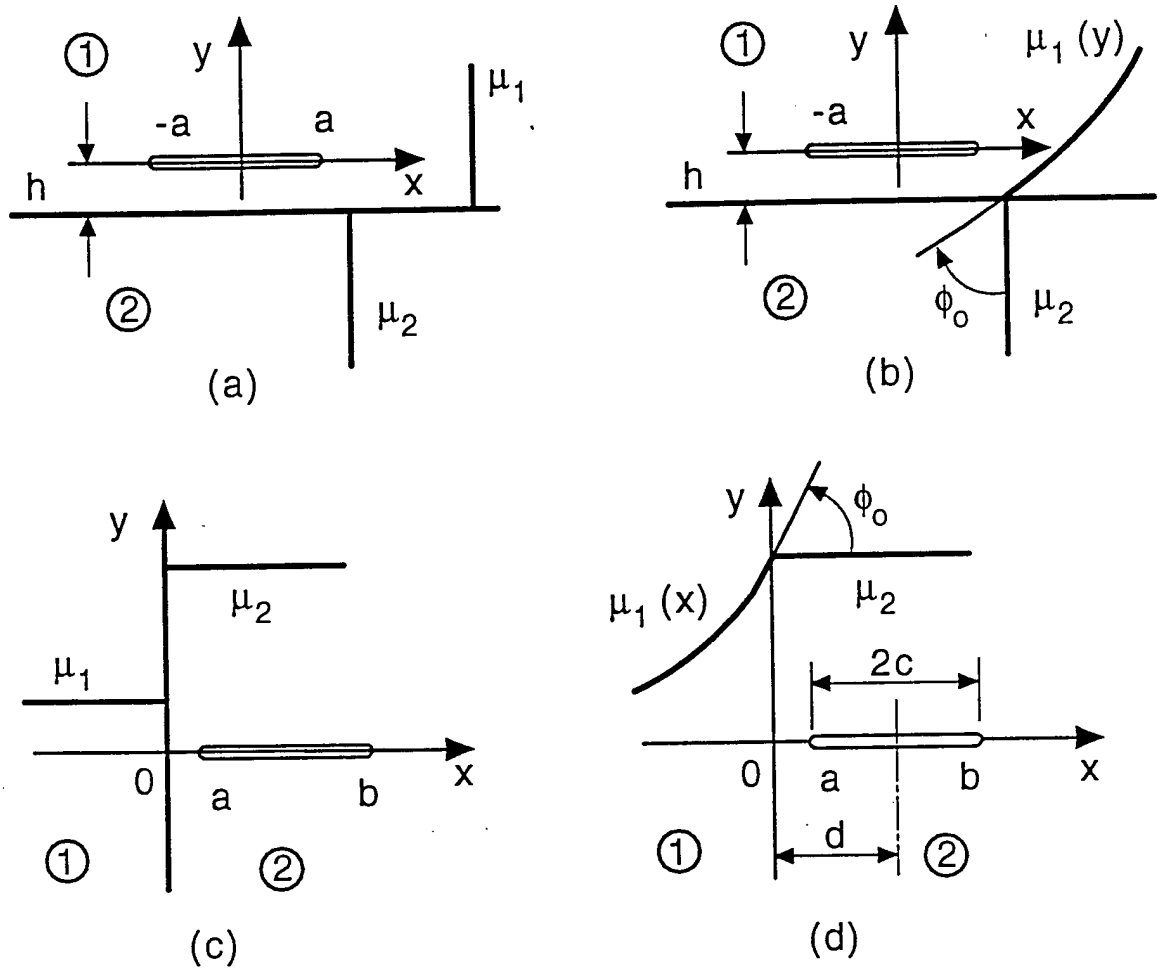

Figure 2: Geometry and notation for a plane crack in bonded homogeneous and nonhomogeneous materials.

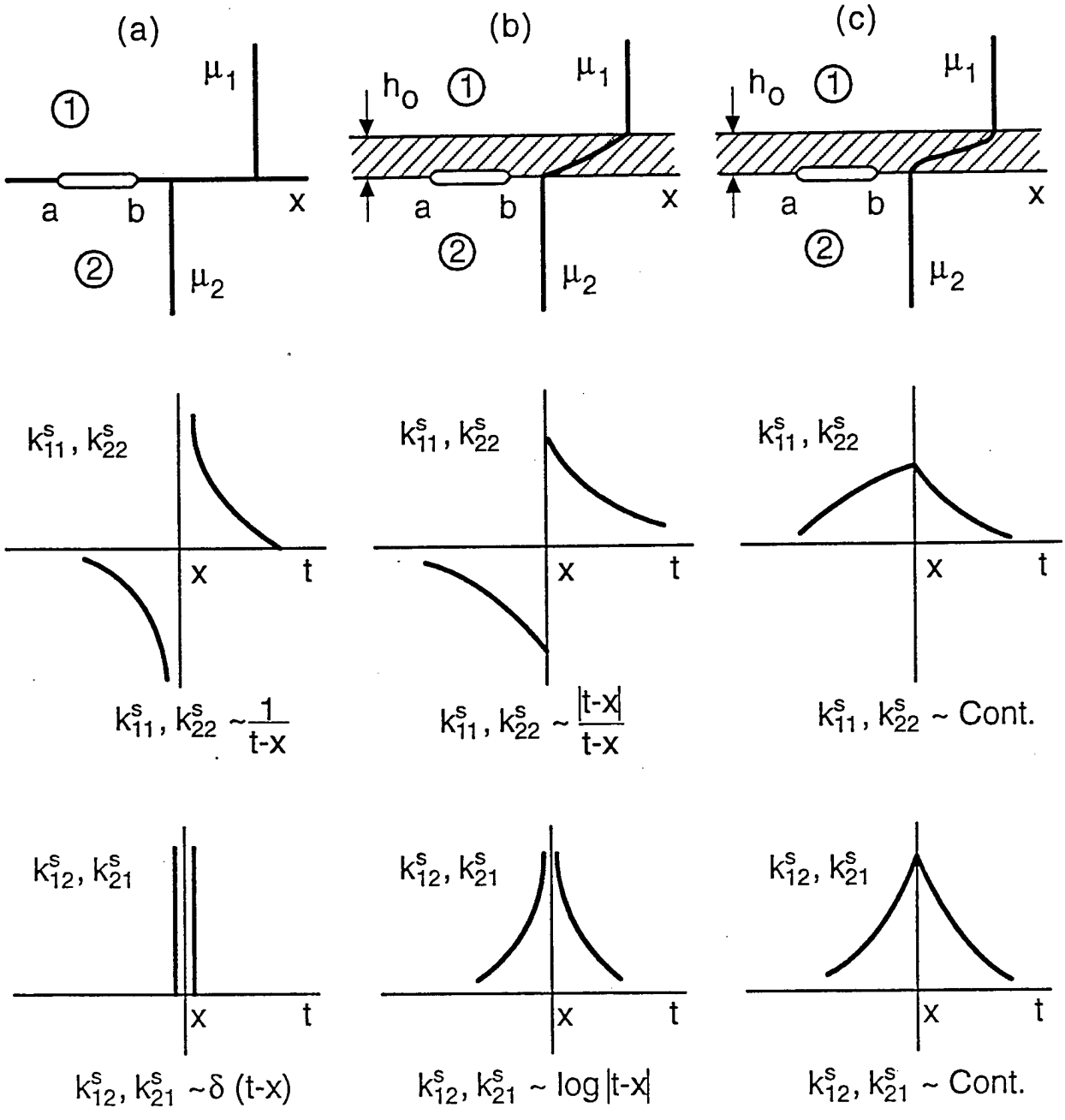

Figure 3: Singular behavior of the irregular kernels for an interface crack in bonded dissimilar materials.

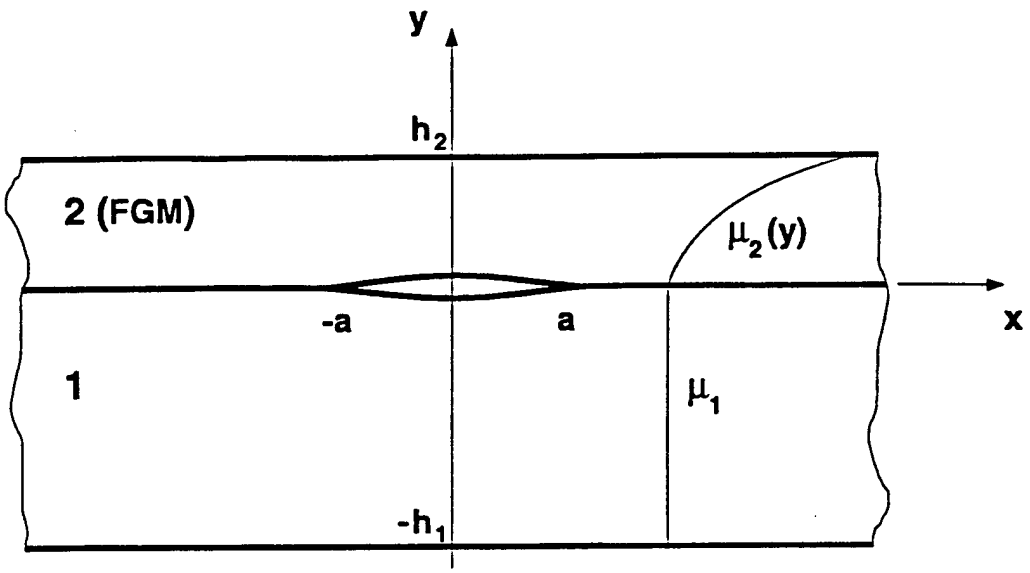

Fig. 4: Geometry of the interface crack for a functionally graded coating bonded to a homogeneous substrate.

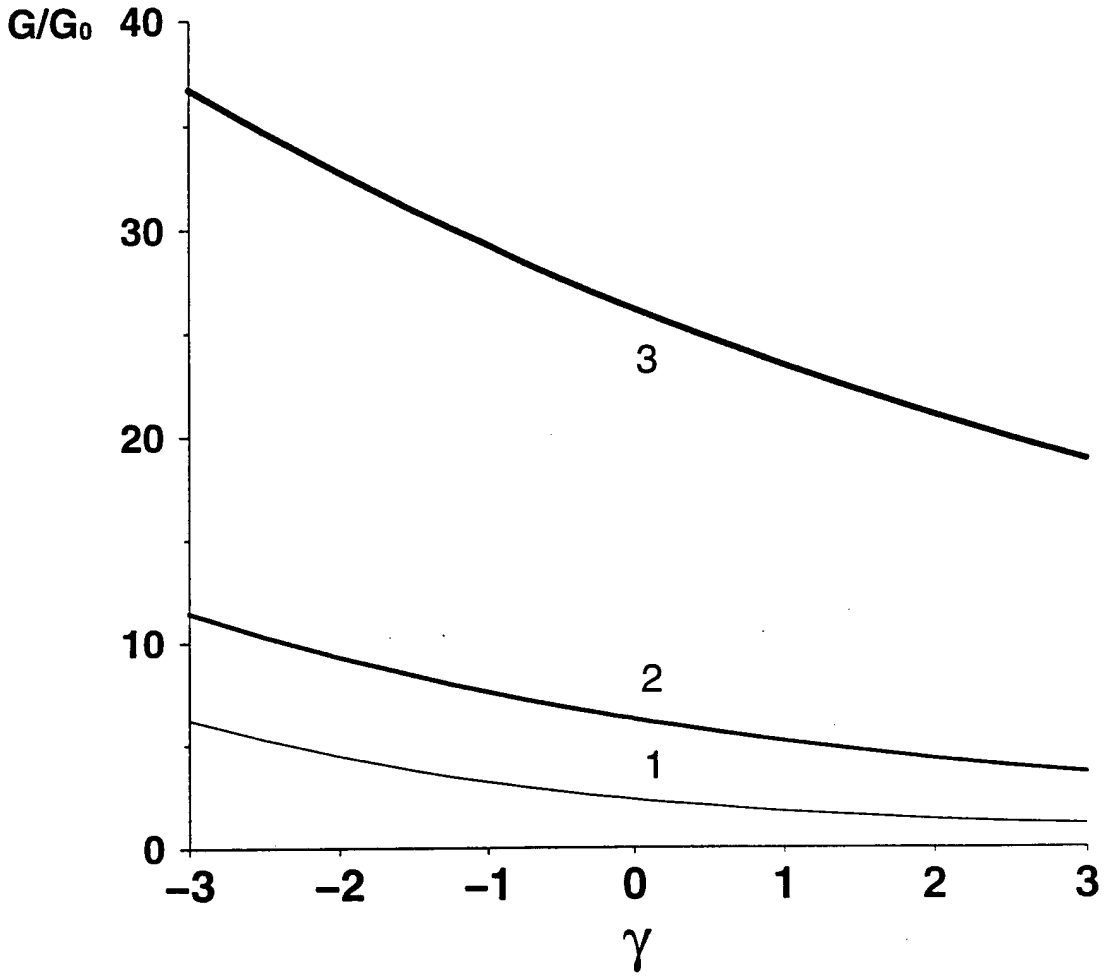

Fig. 5 The influence of h_2 / a on the normalized strain energy release rate $\mathfrak{b}$; loading: uniform crack surface pressure σ_o, ν=0.3, $h_1 / a = 100$, (1) $h_2 / a = 1$, (2) $h_2 / a = 0.5$, (3) $h_2 / a = 0.25$.

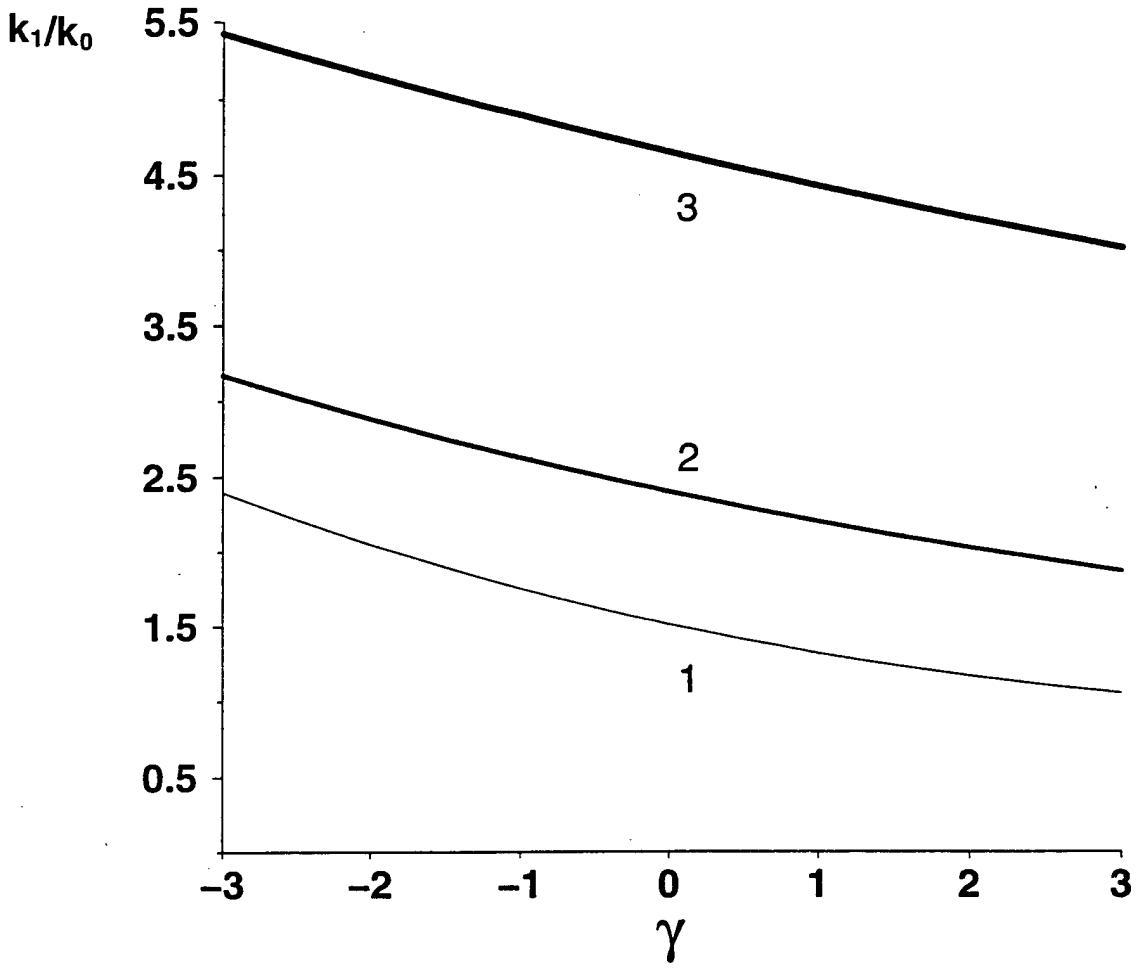

Fig. 6 The influence of h_2 / a on mode I stress intensity factor k_1, loading: σ_o, ν=0.3, $h_1 / a = 100$, (1) $h_2 / a = 1$, (2) $h_2 / a = 0.5$, (3) $h_2 / a = 0.25$.

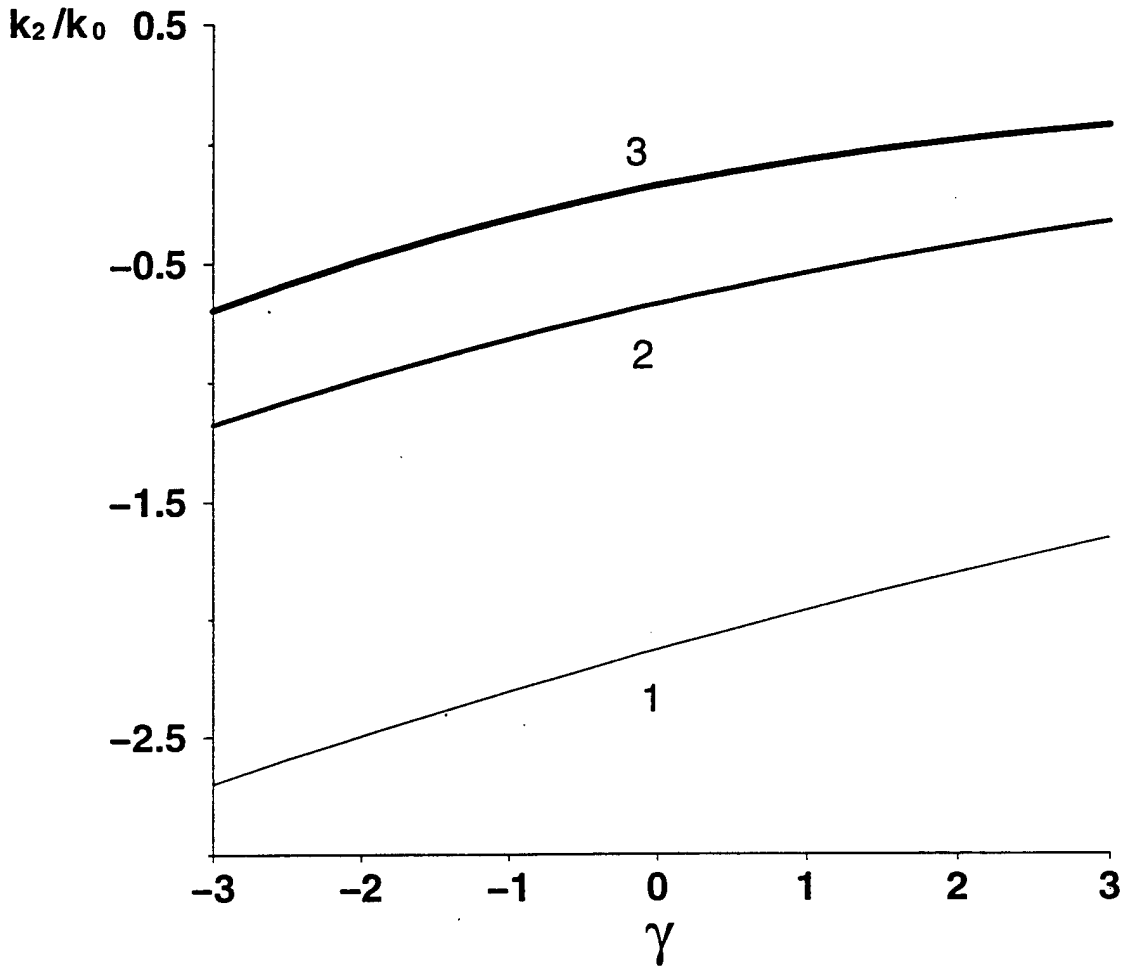

Fig. 7 The influence of h_2 / a on mode II stress intensity factor k_2, loading: σ_o, ν=0.3, $h_1 / a = 100$, (1) $h_2 / a = 0.25$, (2) $h_2 / a = 0.5$, (3) $h_2 / a = 1$.

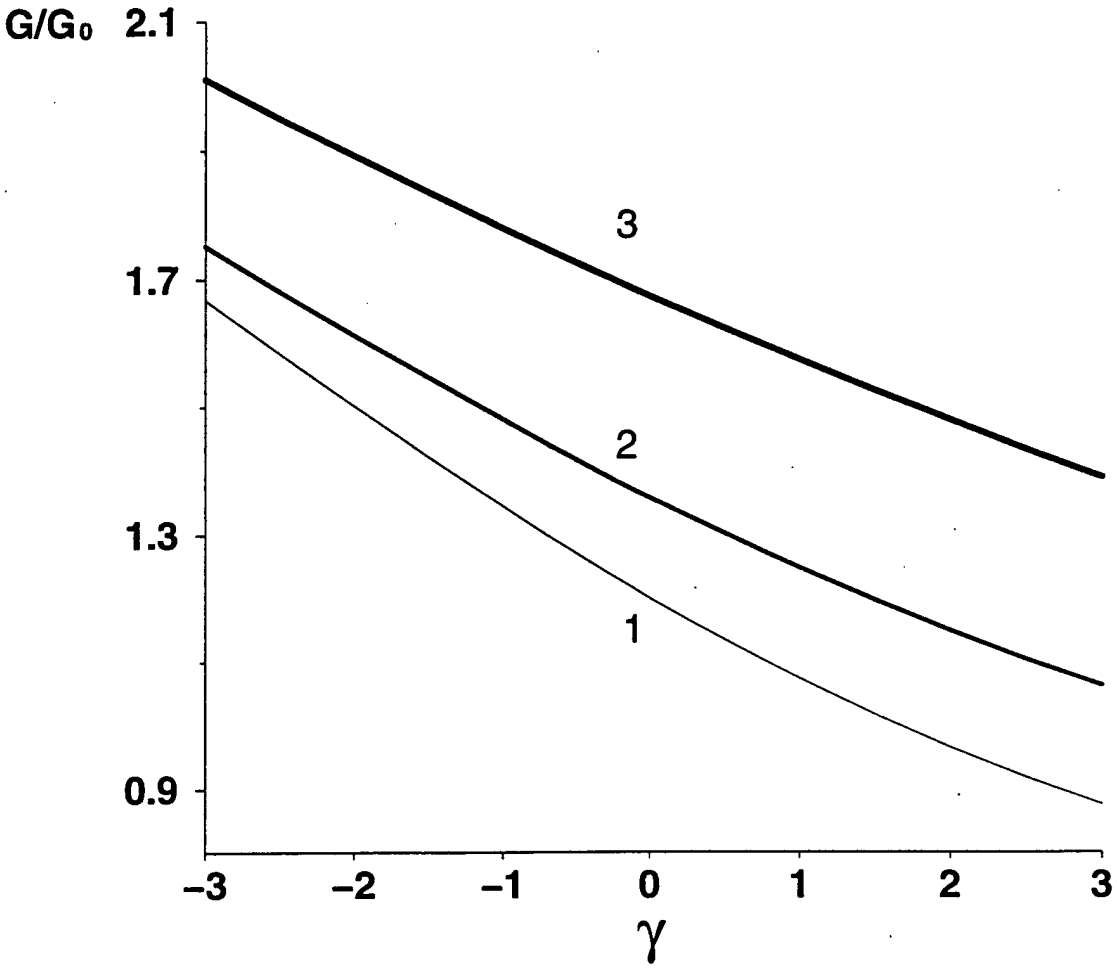

Fig. 8 The influence of h_2 / a on b, loading: uniform crack surface shear τ_o, ν=0.3, $h_1 / a = 100$, (1) $h_2 / a = 1$, (2) $h_2 / a = 0.5$, (3) $h_2 / a = 0.25$.

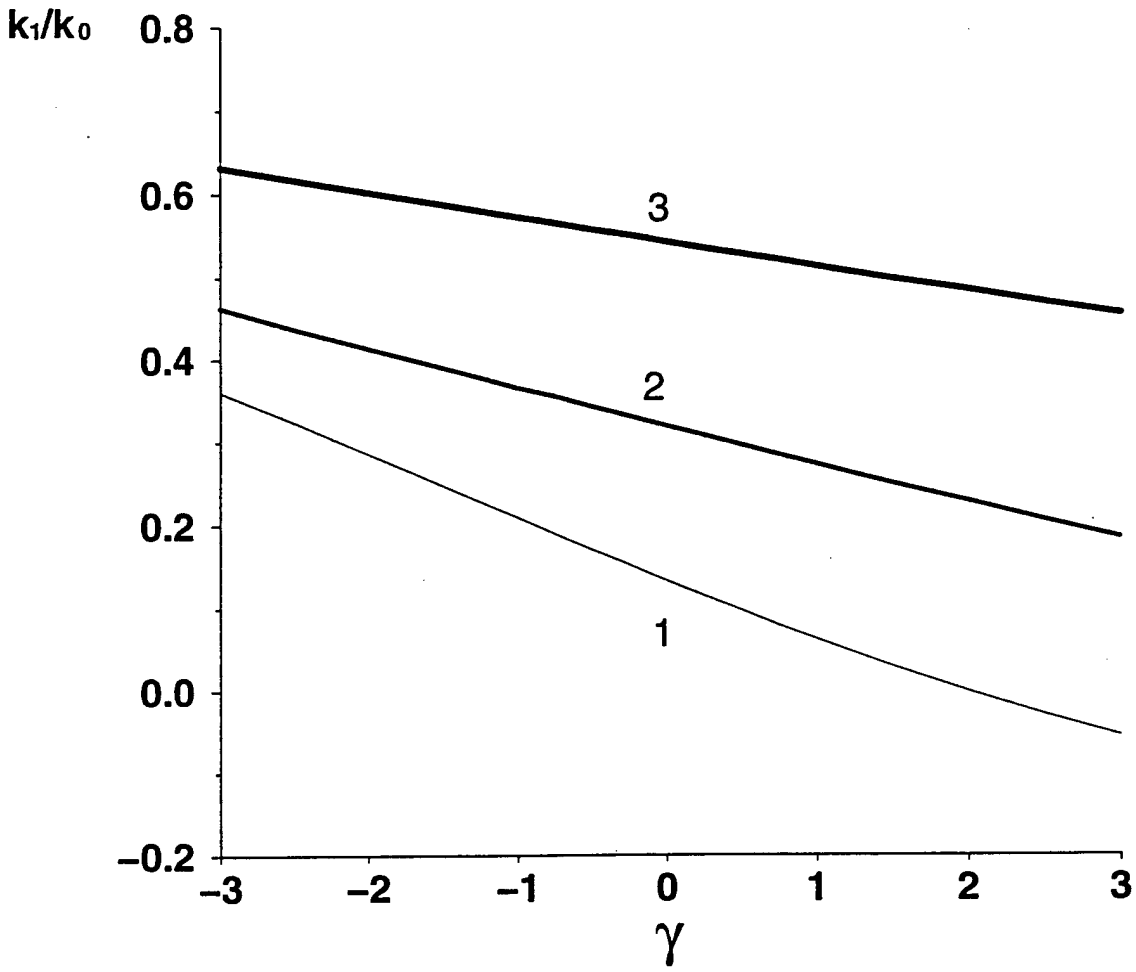

Fig. 9 The influence of h_2 / a on k_1, loading: τ_o, ν=0.3, $h_1 / a = 100$, (1) $h_2 / a = 1$, (2) $h_2 / a = 0.5$, (3) $h_2 / a = 0.25$.

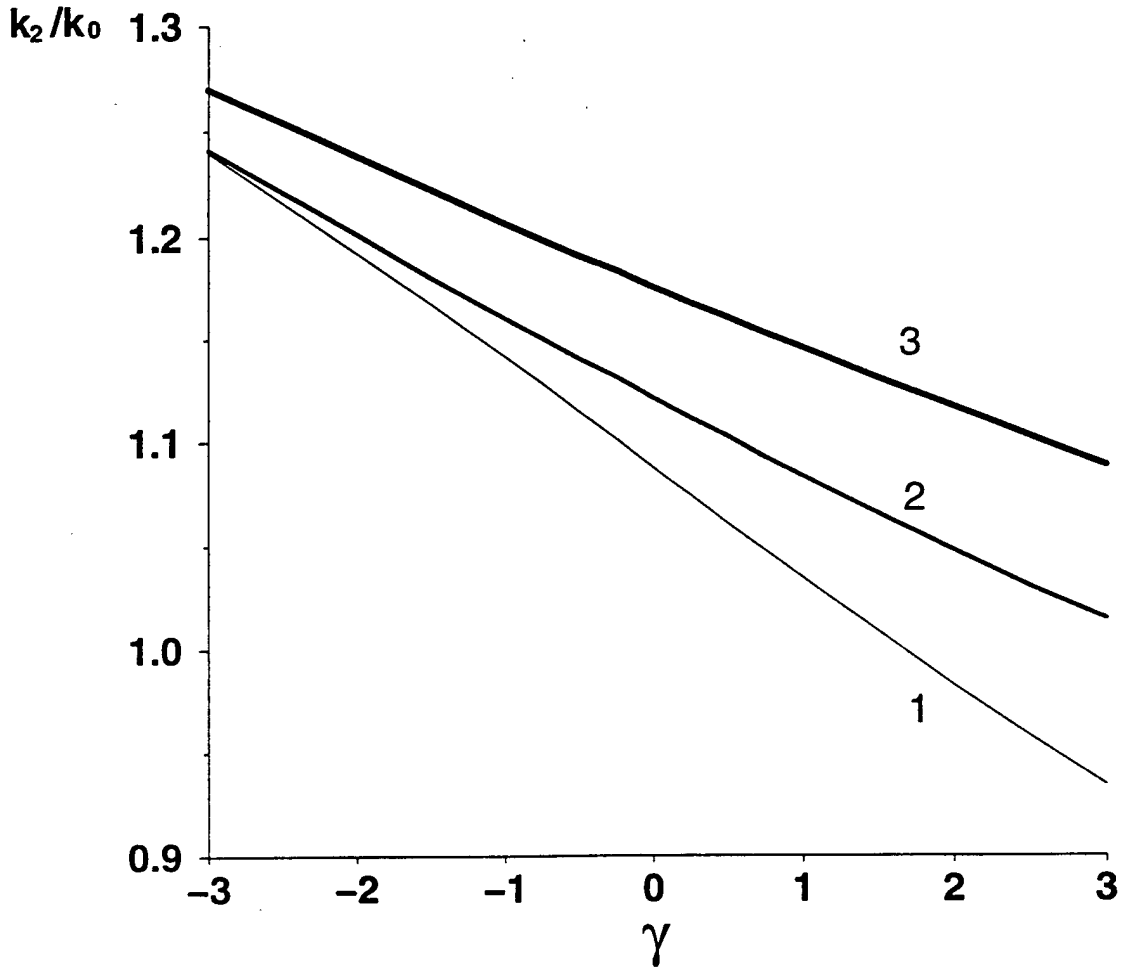

Fig.10 The influence of h_2 / a on k_2, loading: τ_o, ν=0.3, $h_1 / a = 100$, (1) $h_2 / a = 1$, (2) $h_2 / a = 0.5$, (3) $h_2 / a = 0.25$.

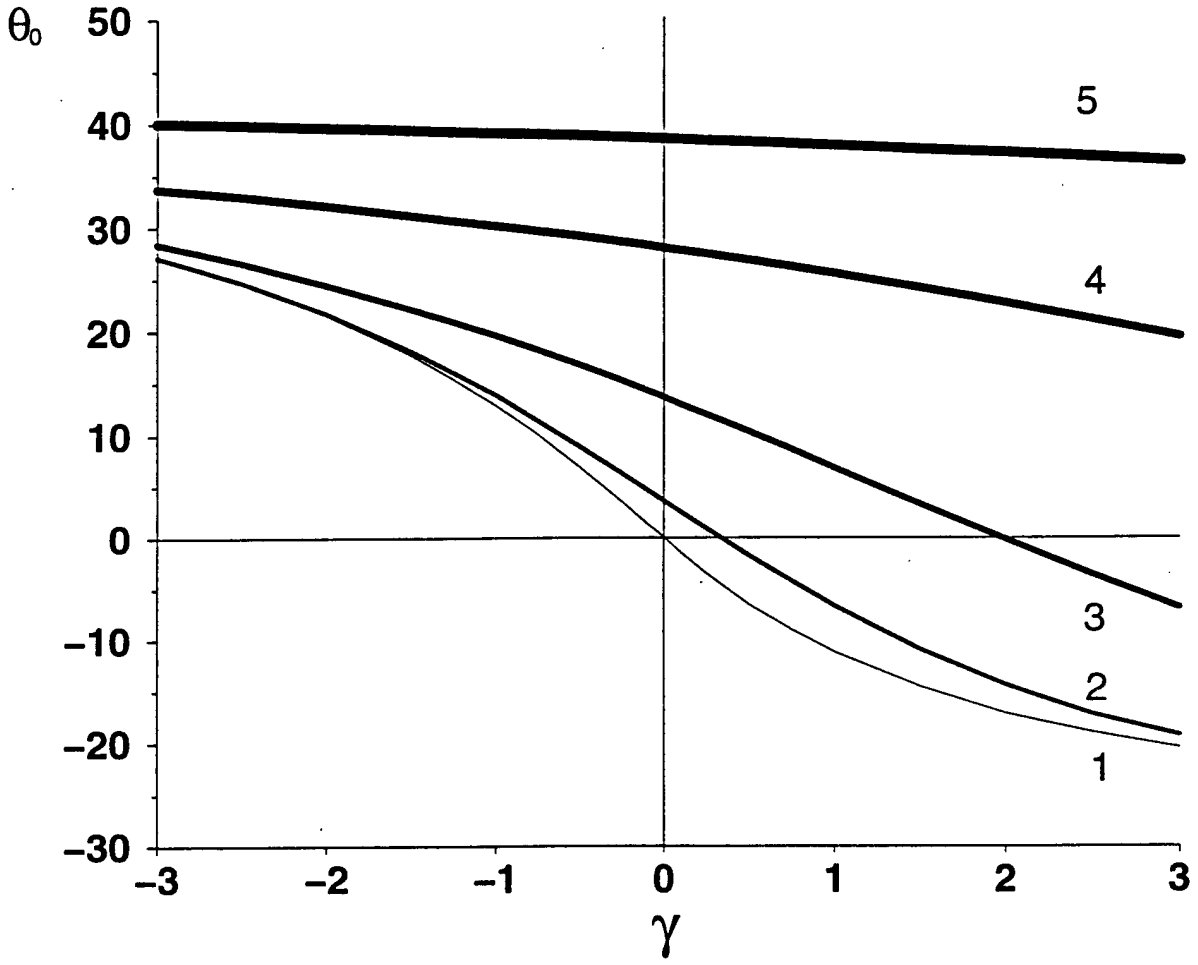

Fig.11 The effect of the coating thickness h_2 / a and the nonhomogeneity constant γ on the probable crack growth direction θ_o, loading: σ_o, ν=0.3, $h_1 / a = 100$, (1) $h_2 / a = 10$ & 100, (2) $h_2 / a = 2$, (3) $h_2 / a = 1$, (4) $h_2 / a = 0.5$, (5) $h_2 / a = 0.25$. (The angle θ_o is measured at the crack tip a from the positive x axis.)

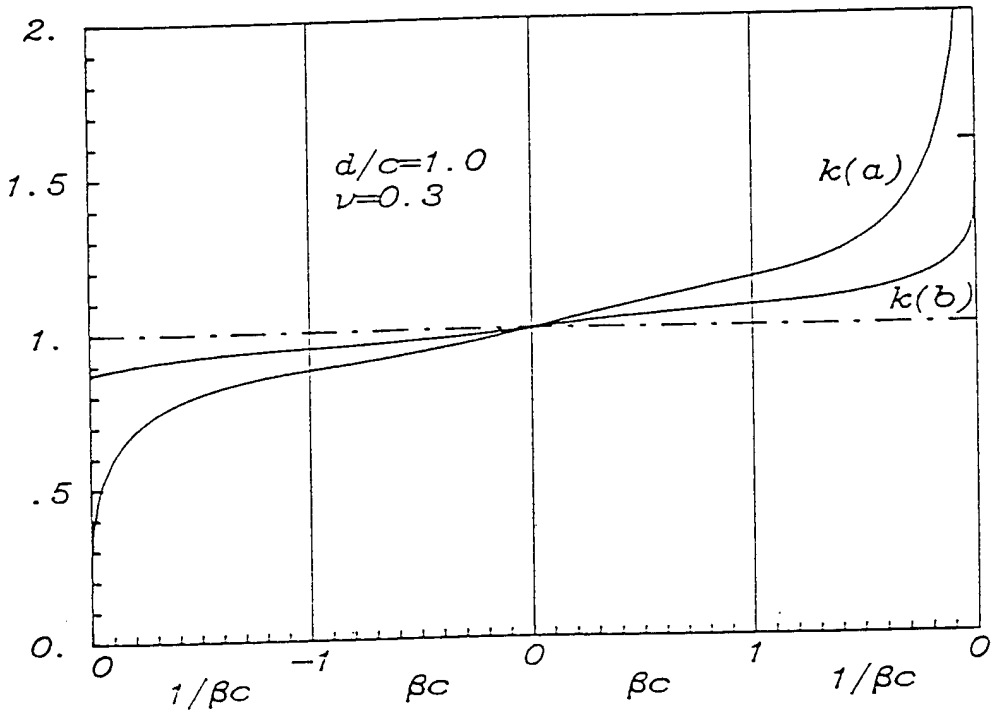

Fig. 12 Normalized stress intensity factors for a plane crack terminating at the interface between a homogeneous medium and a FGM half space.

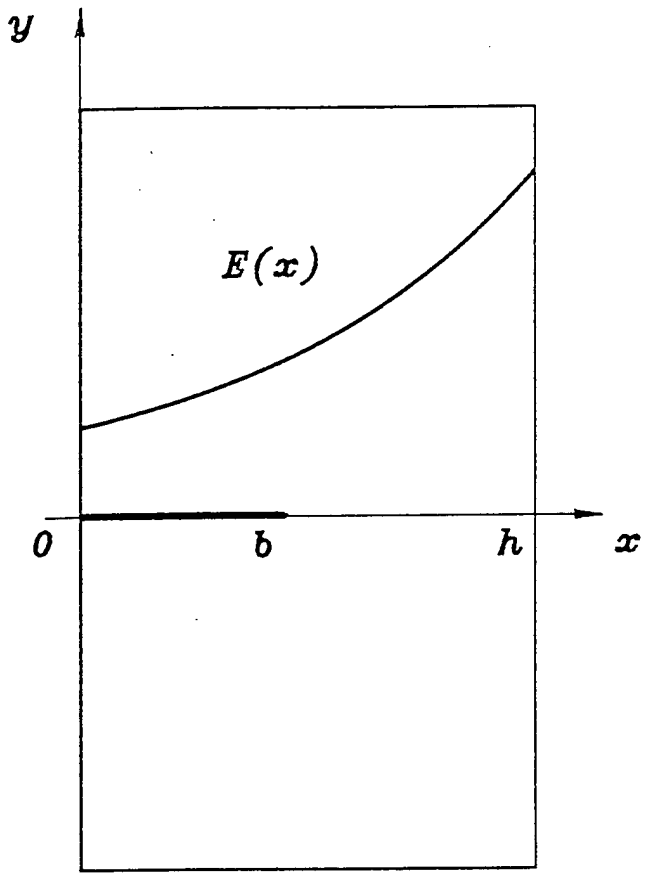

Fig. 13 The geometry of a surface crack in a FGM layer.

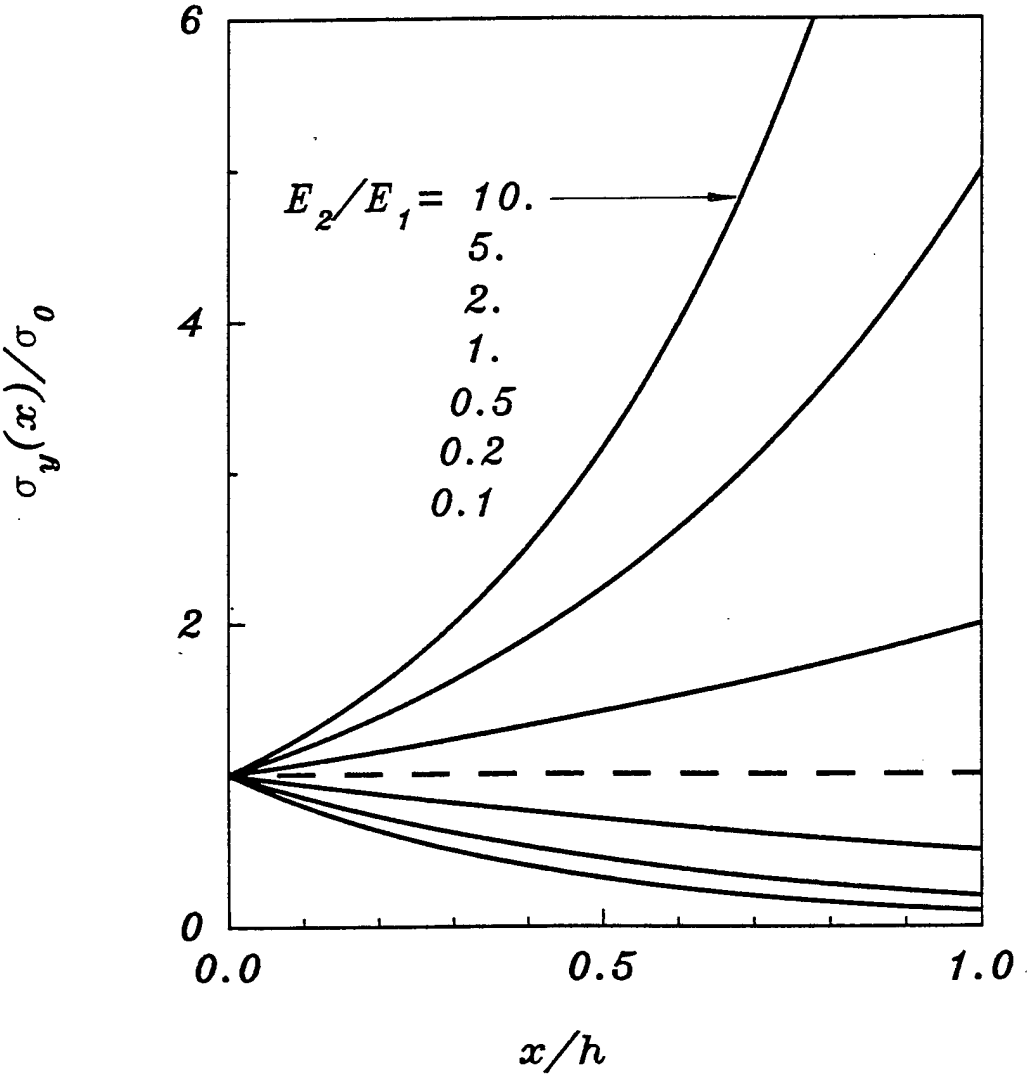

Fig. 14 The stress distribution in the uncracked layer under fixed grip loading $\sigma_0 = \mathrm{E}_1\epsilon_0/(1-\nu^2)$.

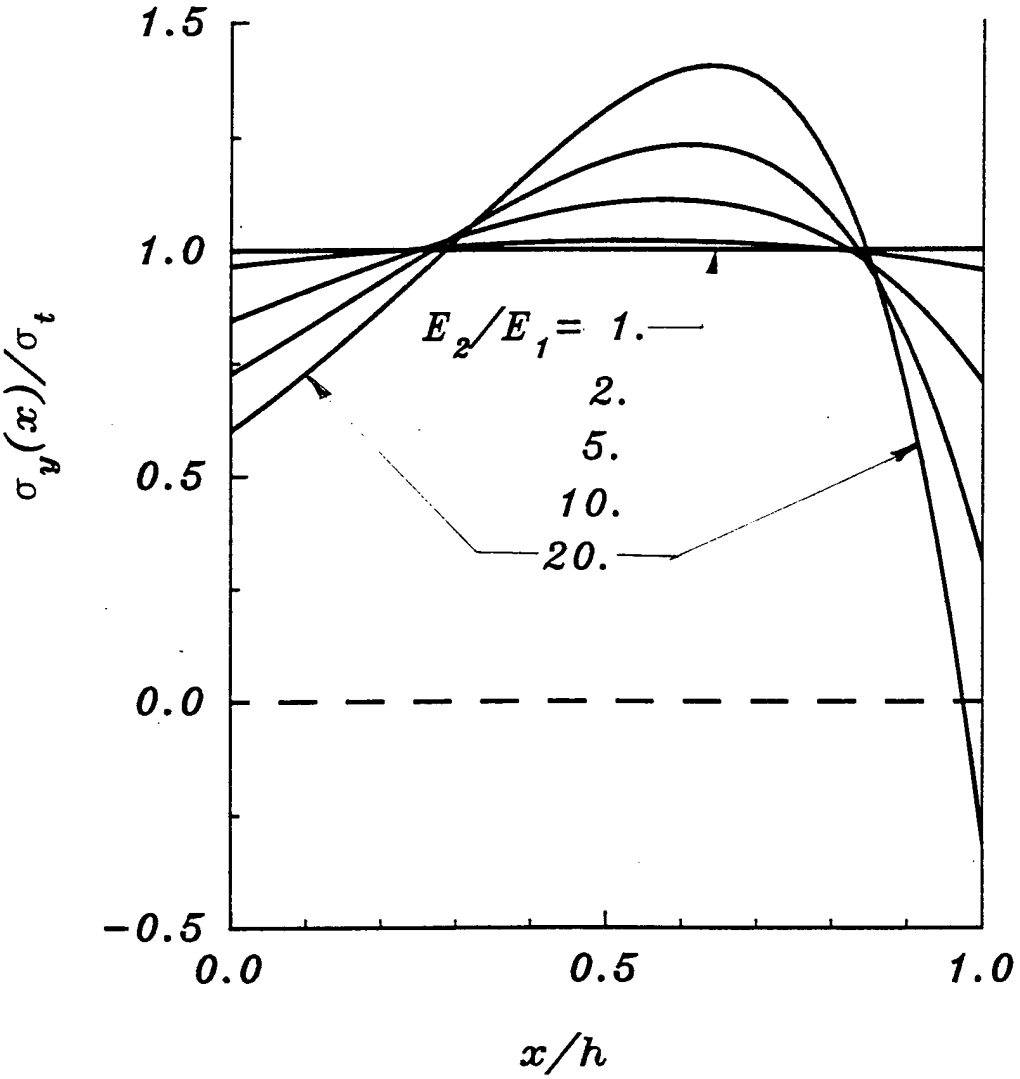

Fig. 15 The stress distribution in the uncracked layer under membrane loading, $\sigma_t = N/h$.

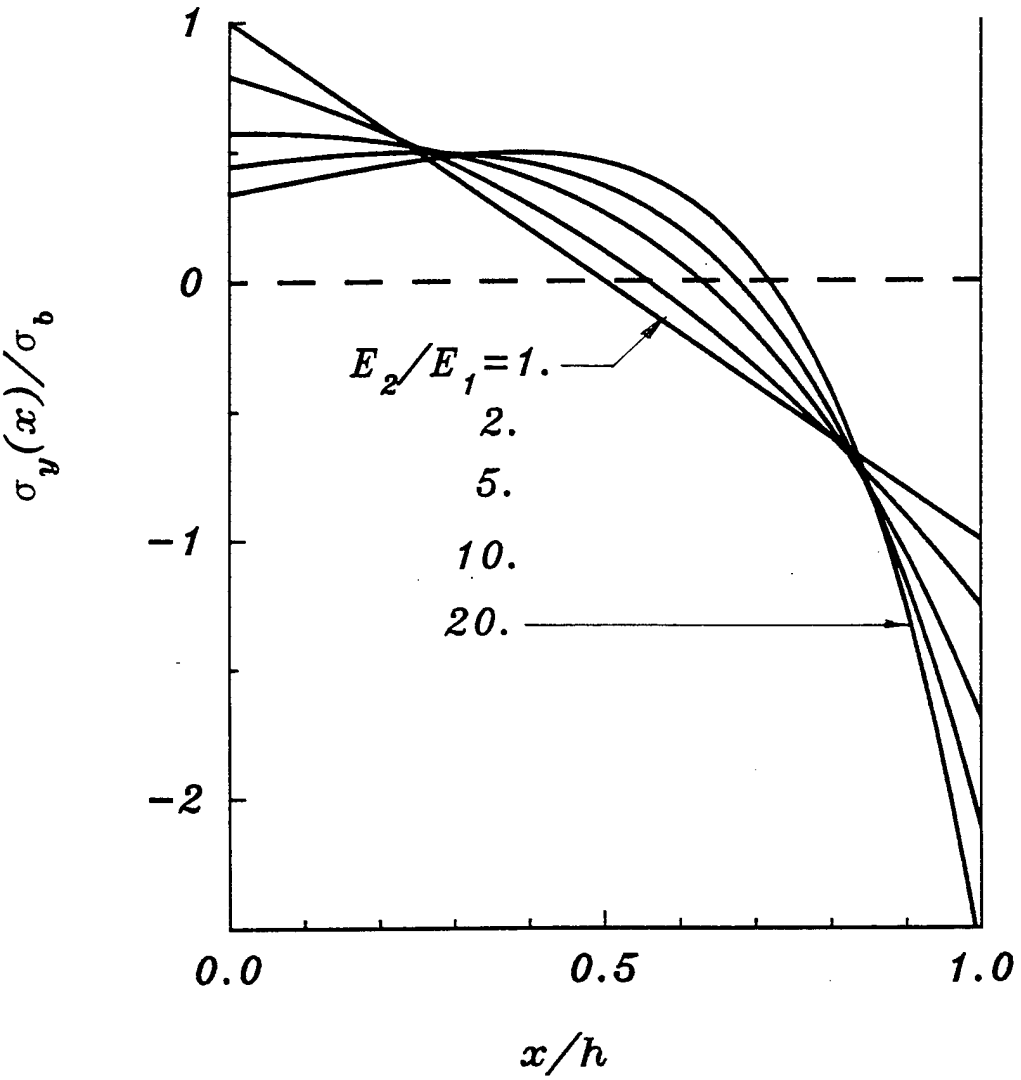

Fig. 16 The stress distribution in the uncracked layer under bending, $\sigma_b = 6M/h^2$.

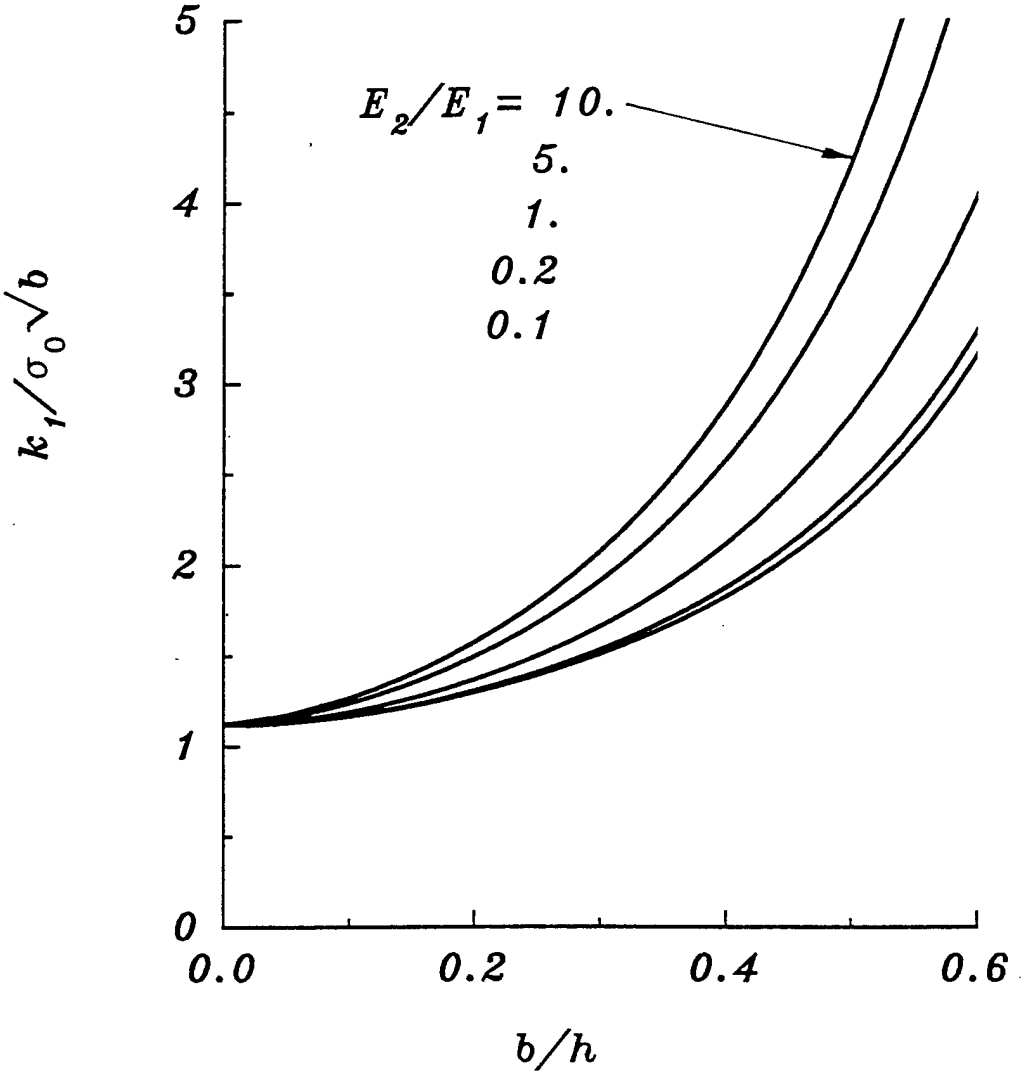

Fig. 17 Stress intensity factor for an edge crack in a graded layer under fixed grip loading, a = 0, $\sigma_0 = \mathrm{E}_1\epsilon_0(1-\nu^2)$.

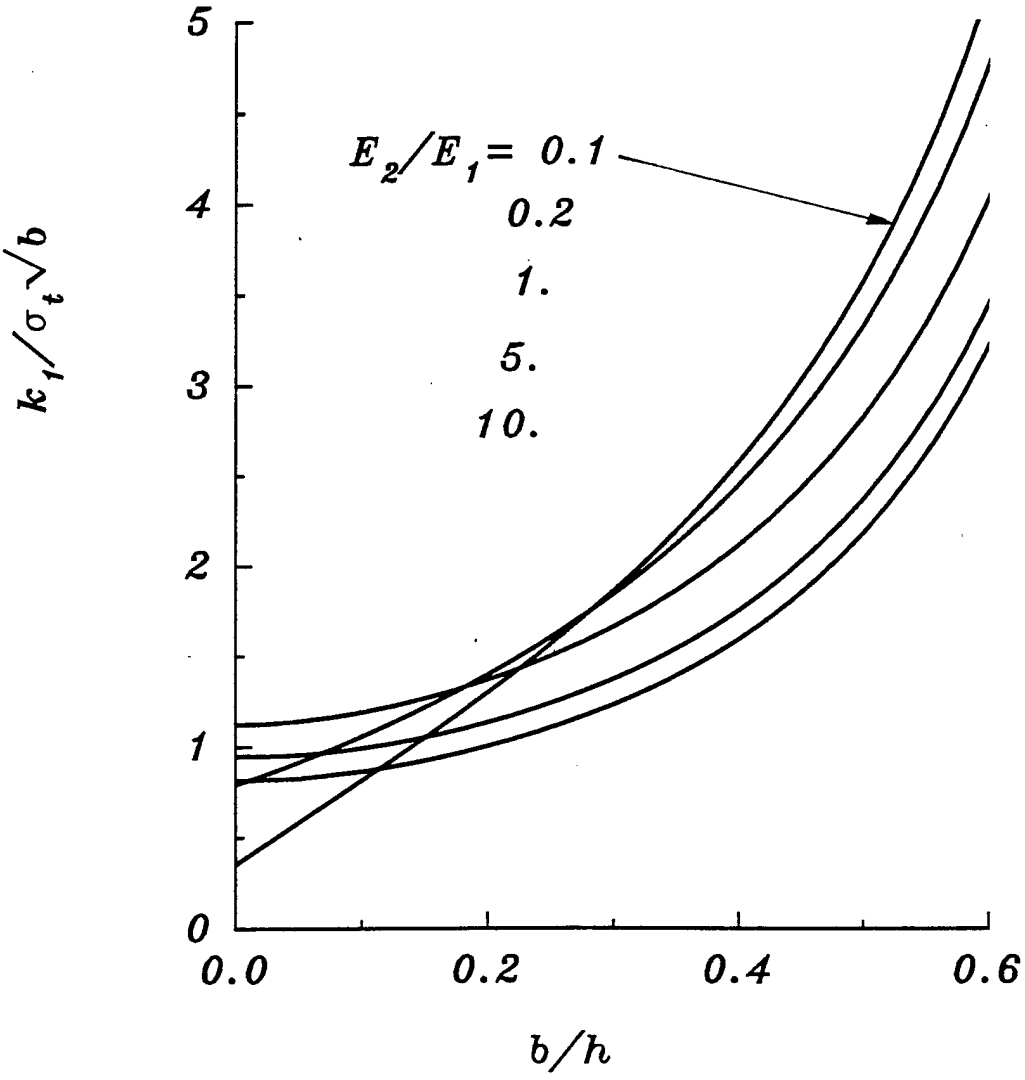

Fig.18 Stress intensity factor for an edge crack in a graded layer under membrane loading, a = 0, σ_t = N/h.

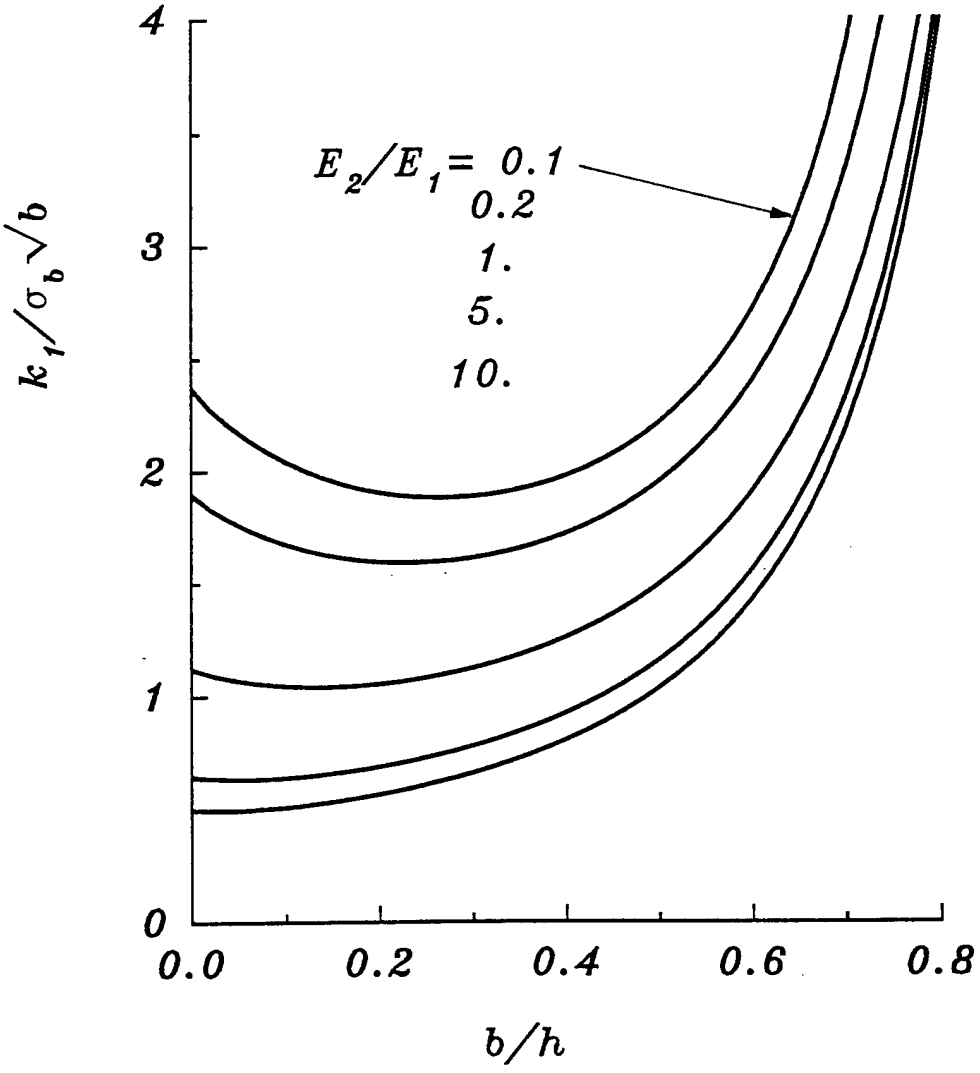

Fig. 19 Stress intensity factor for an edge crack in a graded layer under bending, $a = 0$, $\sigma_b = 6M/h^2$.

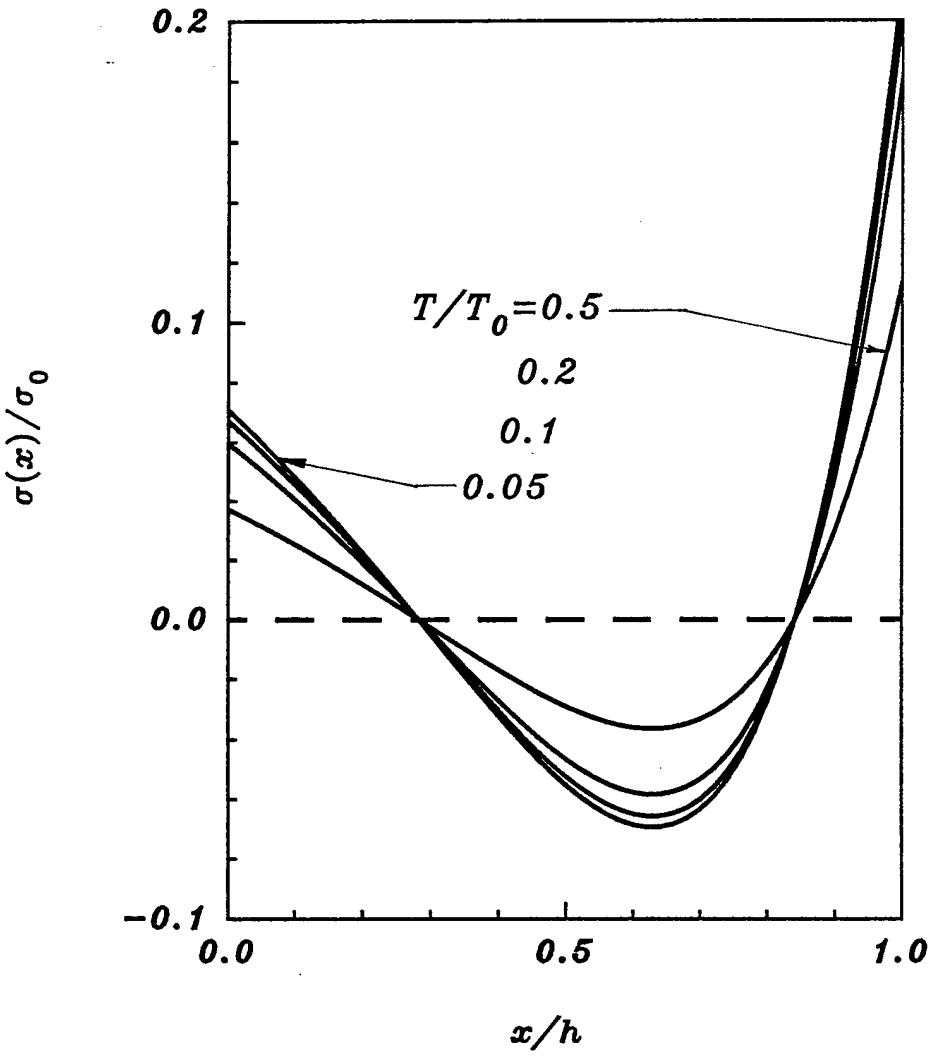

Fig. 20 Thermal stress distribution in a FGM layer with $E_2/E_1=5$, $\alpha_2/\alpha_1=2$, undergoing a uniform temperature change, $T_1=T_2=T$, $T<T_o$.

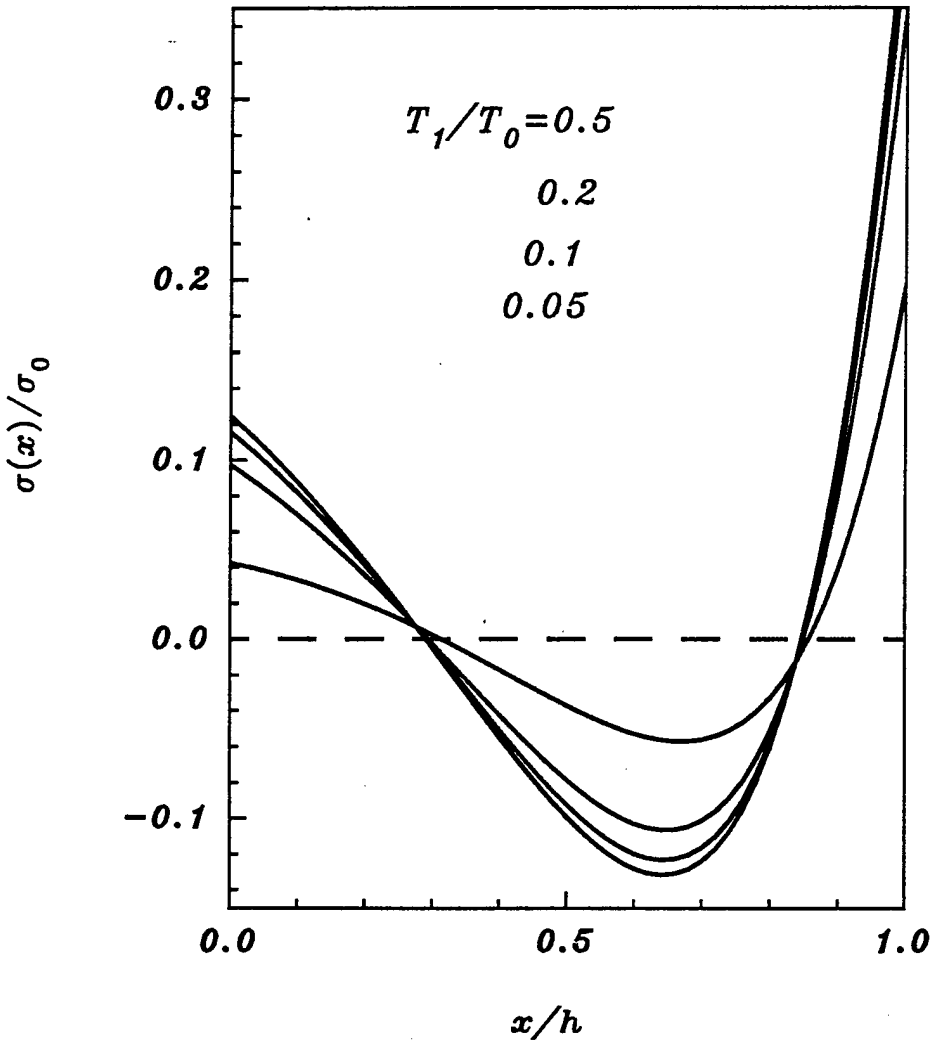

Fig. 21 Thermal stress distribution in a FGM layer with E_2/E_1=10, α_2/α_1=2, λ_2/λ_1=10, under steady-state heat conduction; $T(h)=T_2=0.5T_o$, $T(0)=T_1$ variable.

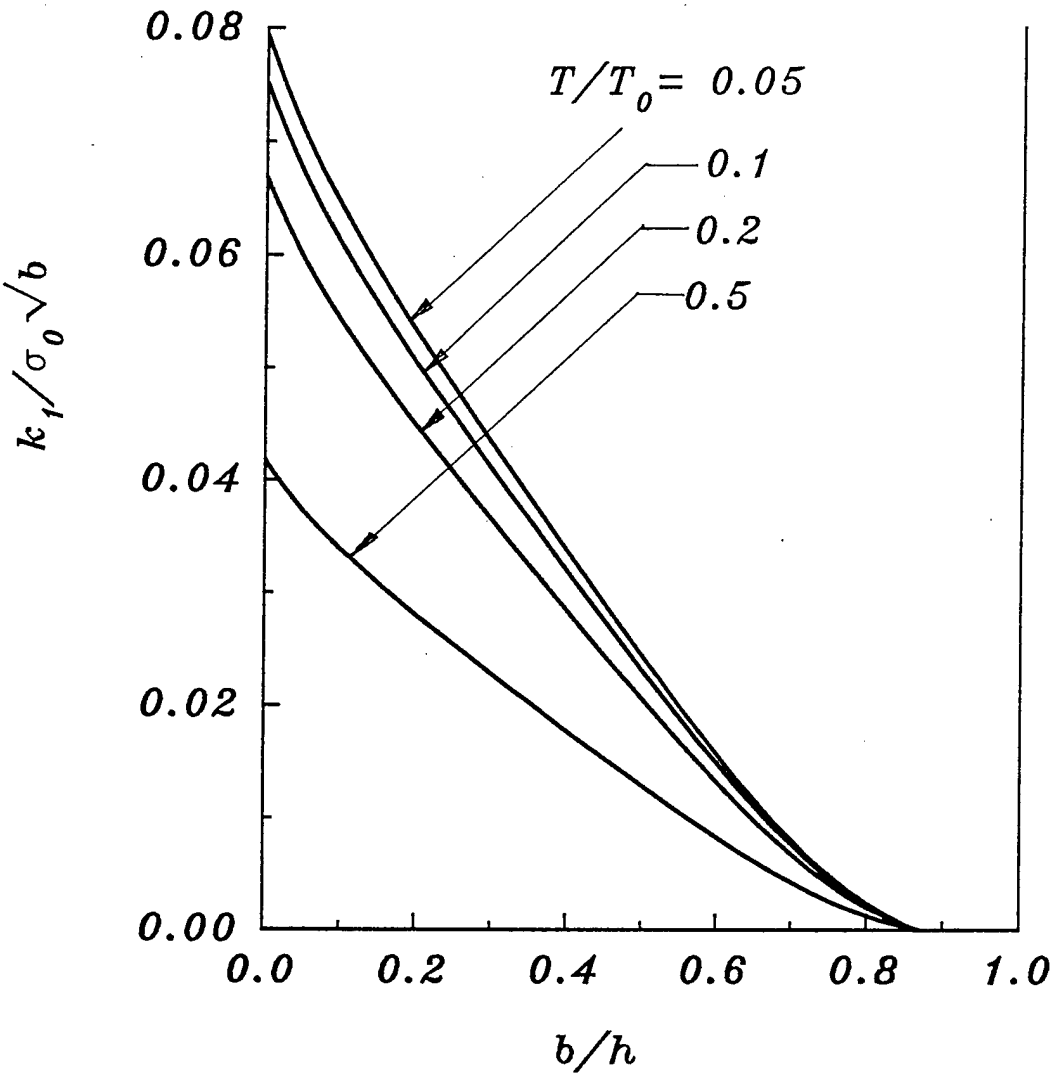

Fig. 22 Normalized Stress intensity factor $k_1(b)/\sigma_0\sqrt{b}$ for a surface crack in a FGM layer under the stress state shown in Fig. 20 (E_2/E_1=5, α_2/α_1=2).

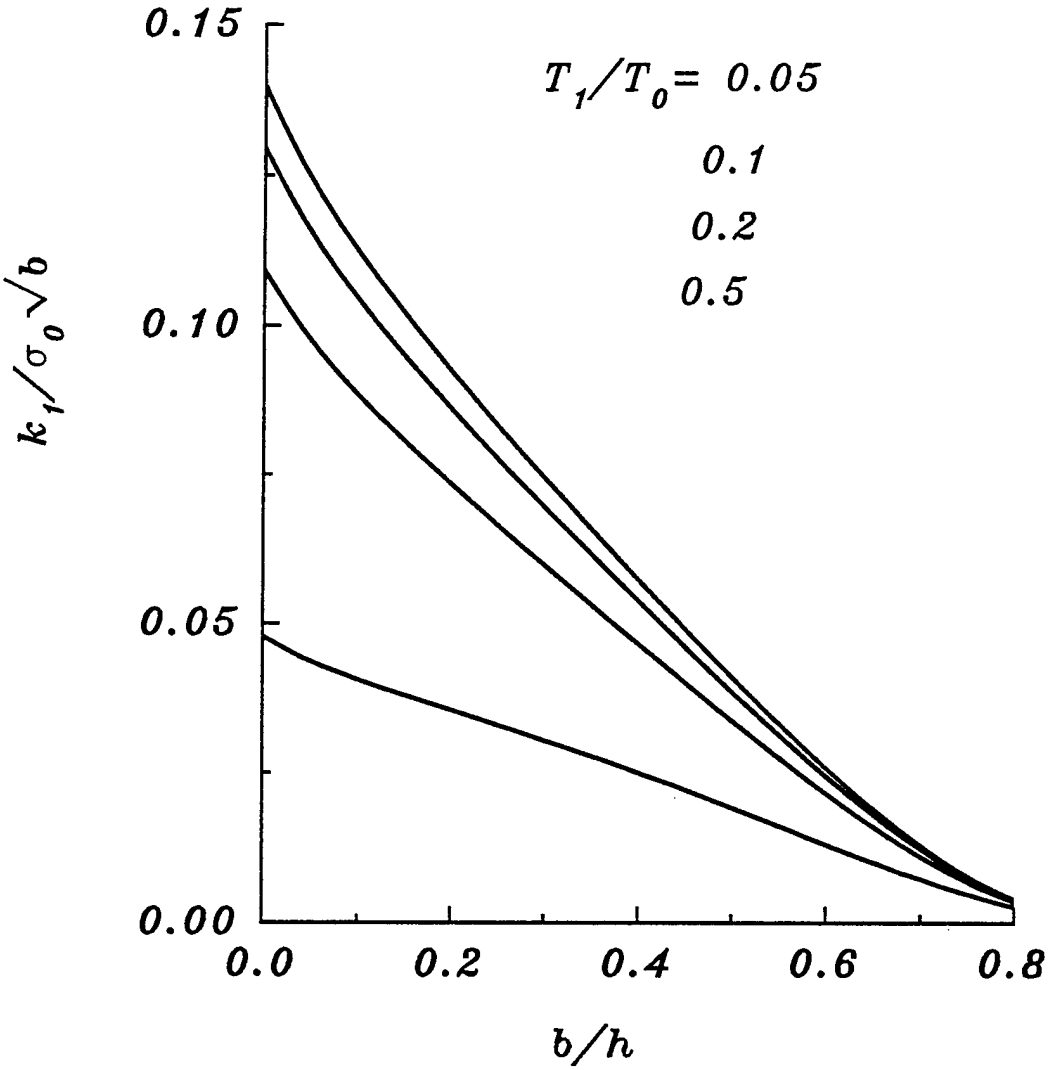

Fig. 23 Normalized stress intensity factor for a surface crack in a FGM layer under the stress state shown in Fig. 21 (E_2/E_1=10, α_2/α_1=2, λ_2/λ_1=10).

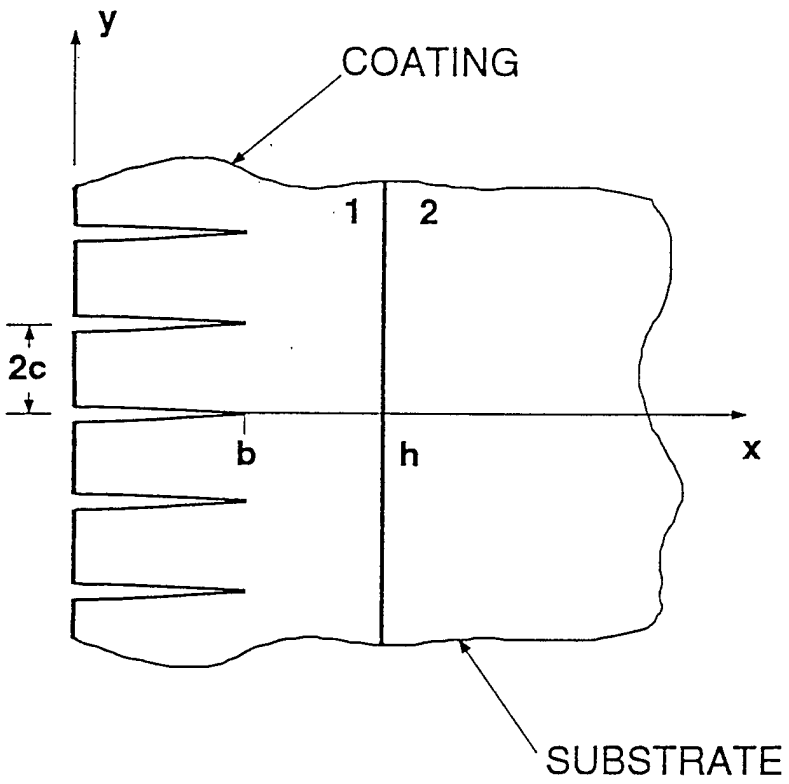

Fig. 24 Geometry of periodic surface cracks in a FGM coating on a homogeneous substrate.

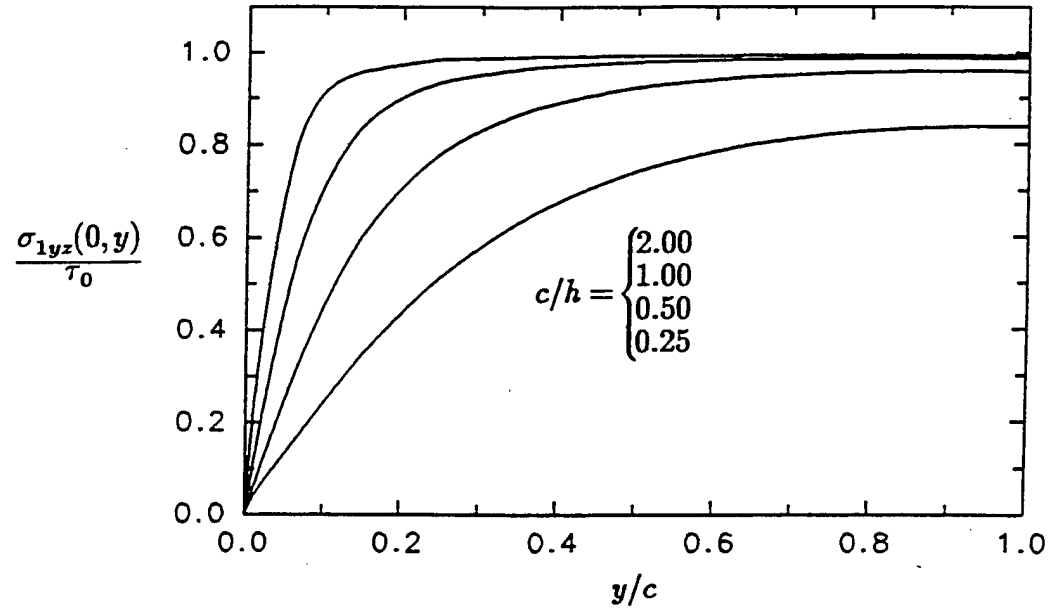

Fig. 25 The stress $\sigma_{1yz}(0,y)$ on the surface of a periodically cracked FGM coating bonded to a homogeneous medium under remote constant shear strain γ_0; $\beta h = 0.5$, $b/h = 0.1$, $\tau_0 = \gamma_0 \mu_1(0)$.

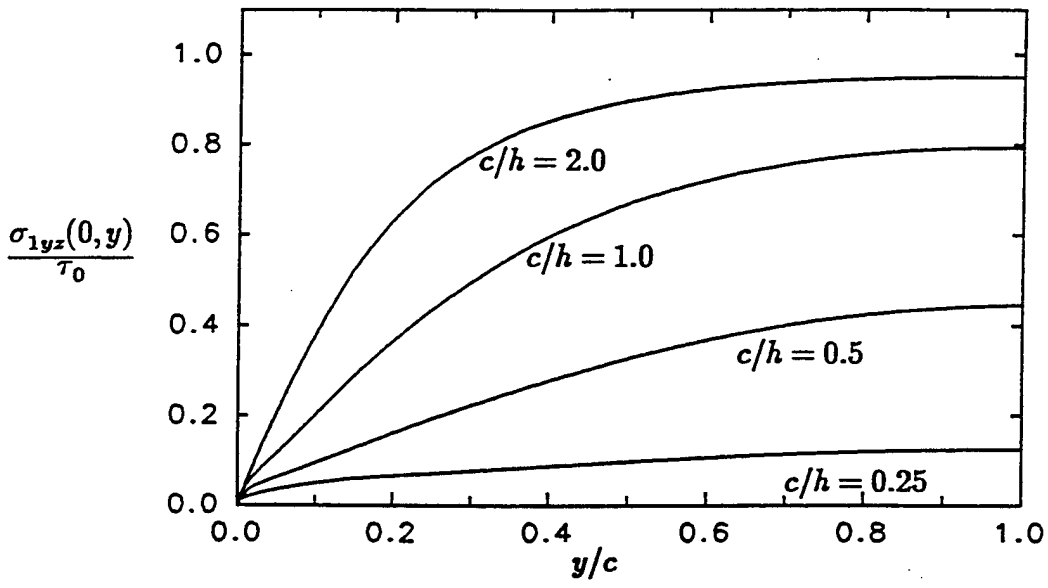

Fig. 26 Same as Figure25 $\beta h = 0.5$, $b/h = 0.5$, $\tau_0 = \gamma_0 \mu(0)$.

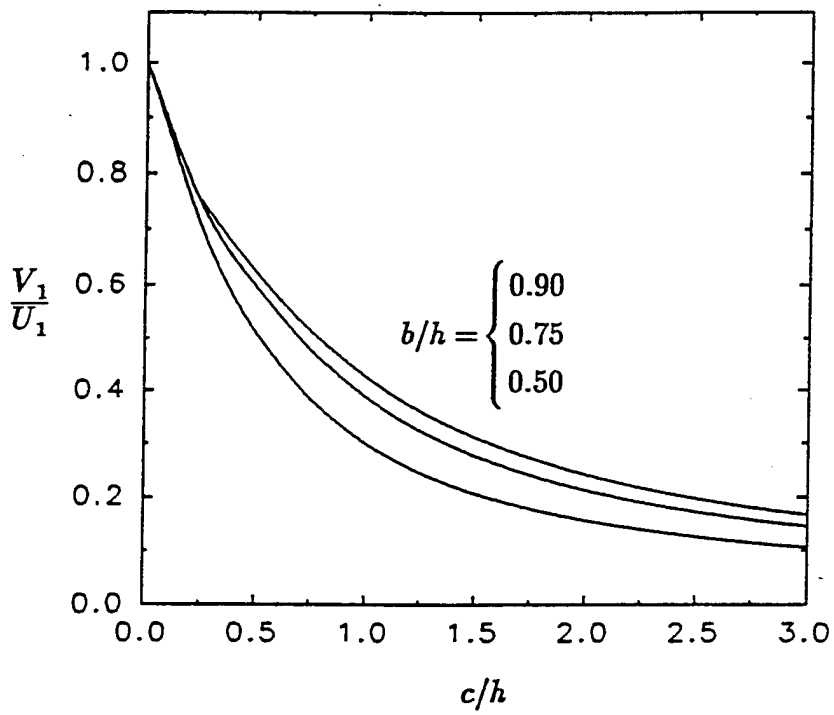

Fig. 27 Released strain energy per unit surface area of a periodically cracked FGM coating bonded to a homogeneous substrate under constant strain loading γ_0; $\beta h = 1.0$, $U_1 = (1/2)\mu_1(0)\gamma_0^2(e^{\beta b} - 1)/\beta$.

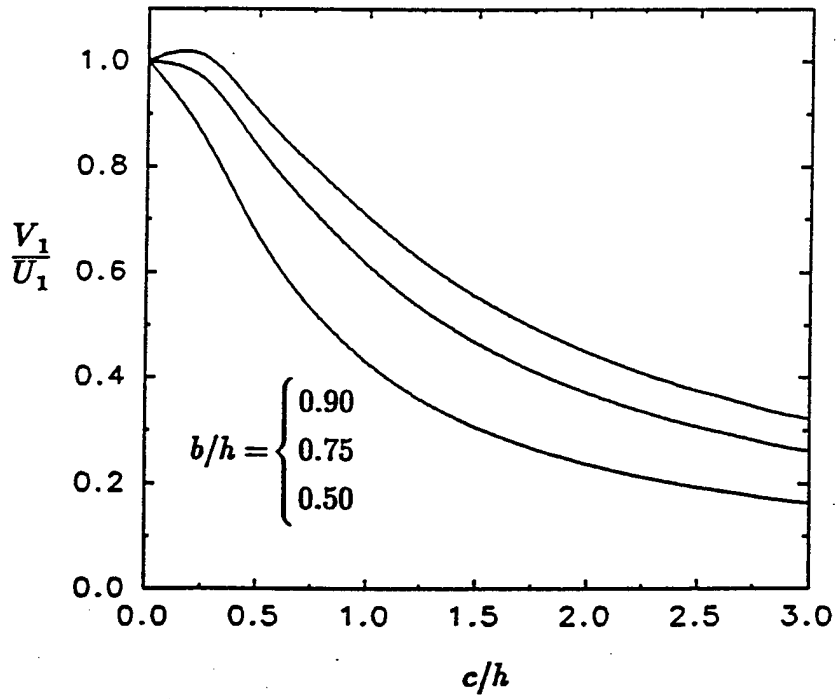

Fig. 28 Same as Figure 27 $\beta h = -1.0$, $U_1 = \frac{1}{2}\mu_1(0)\gamma_0^2(e^{\beta b} - 1)/\beta$.

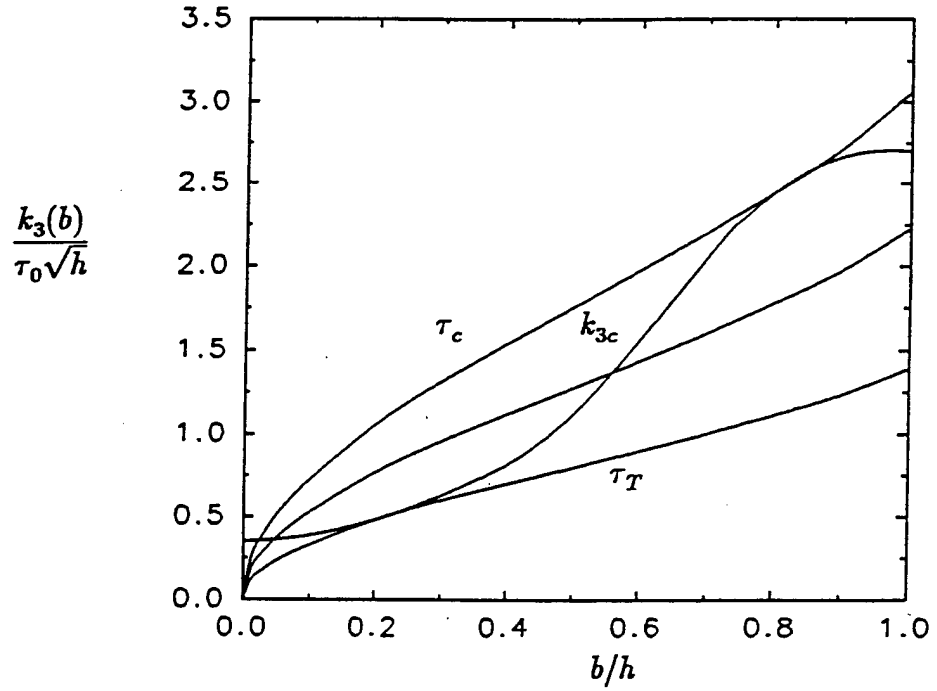

Fig. 29 Fracture instability for periodic cracks in a FGM coating on a homogeneous medium under constant strain γ_0; $\beta h = 1.0$, $c/h = 0.5$, $\tau_0 = \gamma_0\mu_1(0)$.

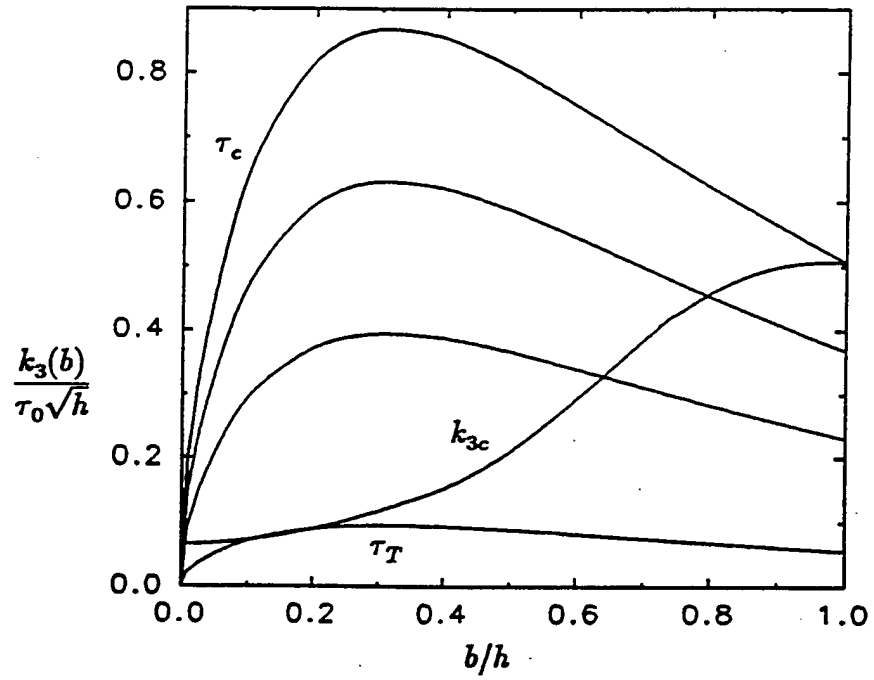

Fig. 30 Same as Figure 29 $\beta h = -1.0$, $c/h = 0.5$, $\tau_0 = \gamma_0\mu(0)$.

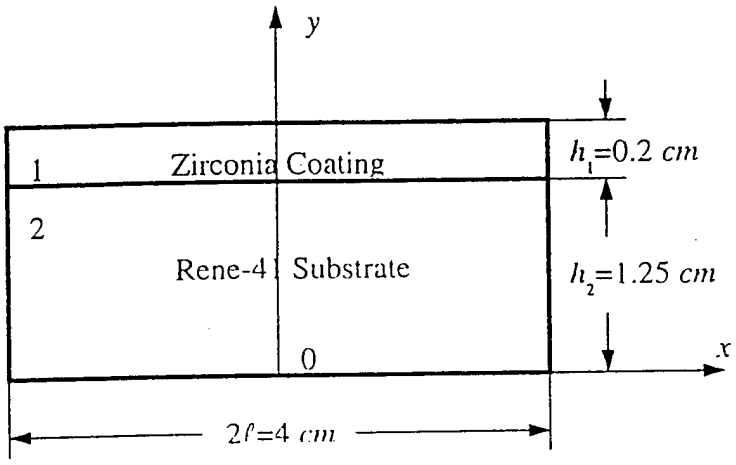

Fig. 31 The geometry of the coating/substrate considered as an example.

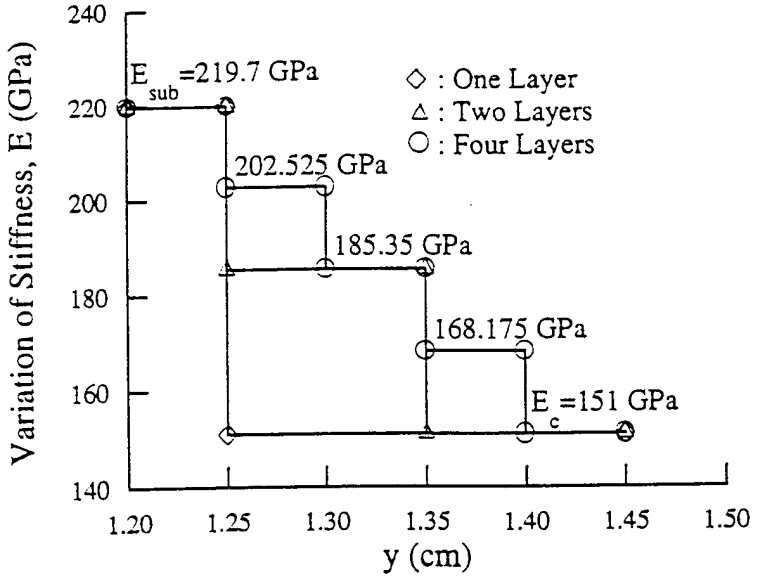

Fig. 32 Stepwise distribution of the elastic modulus for a single, two and four layer homogeneous coatings.

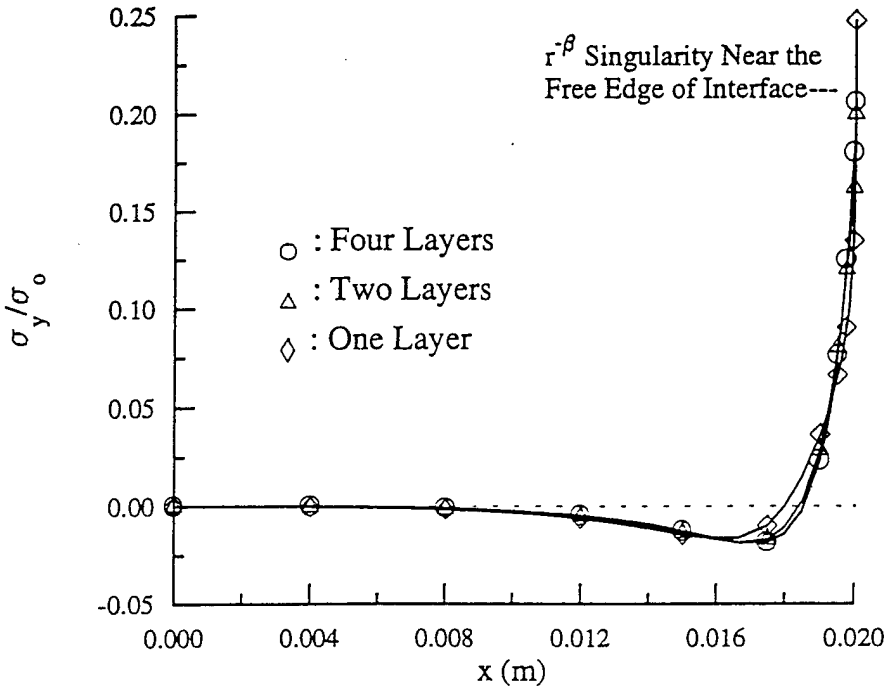

Figure 33 Variation of normalized σ_y along the 1st interface of laminated homogeneous coating; $\sigma_0 = E_s\alpha_s\Delta T$.

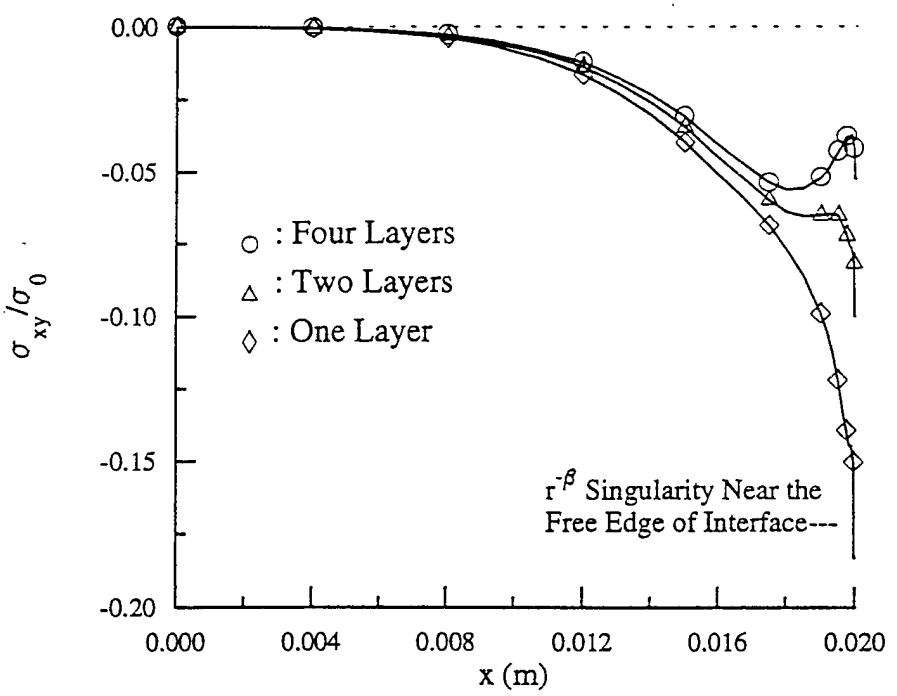

Figure 34 Variation of normalized σ_{xy} along the 1st interface of laminated homogeneous coatings; $\sigma_0 = E_s\alpha_s\Delta T$.

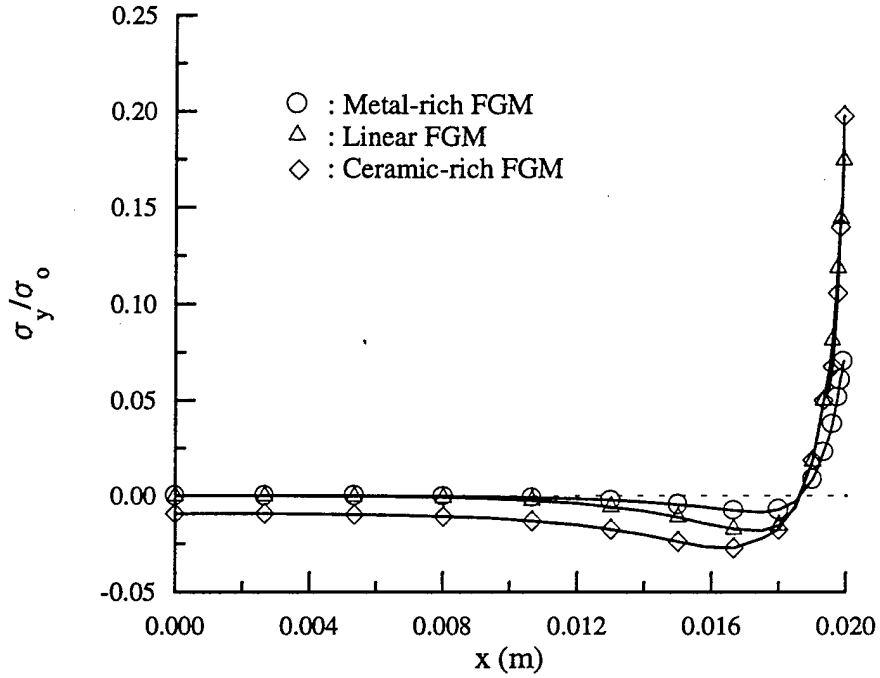

Figure 35 Variation of normalized σ_y along the interface y=0.0125m for FGM coatings; $\sigma_0 = E_s\alpha_s\Delta T$.

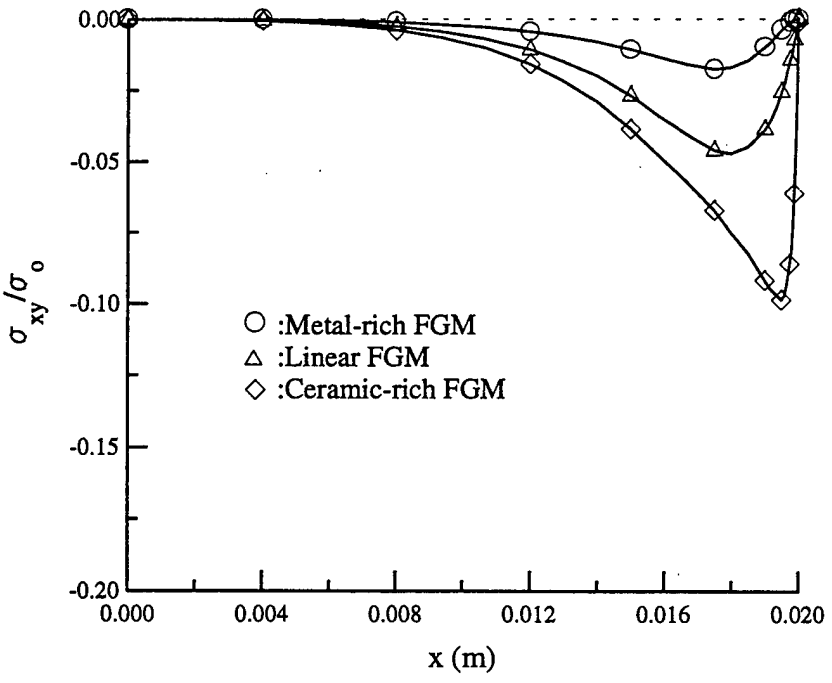

Figure 36 Variation of normalized σ_{xy} along the interface y=0.0125m for FGM coatings; $\sigma_0 = E_s\alpha_s\Delta T$.

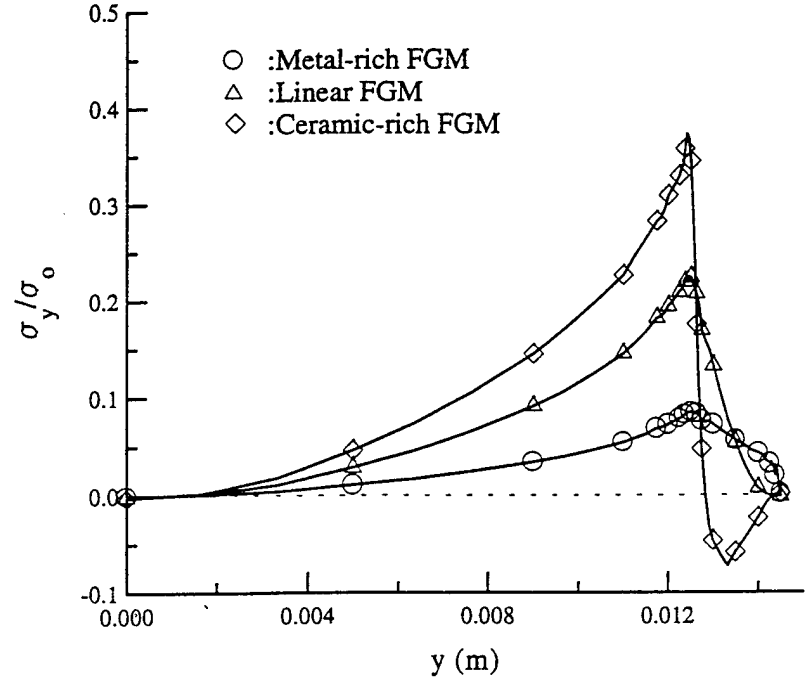

Figure 37 Variation of normalized σ_y along the end $x = \ell = 0.02m$ for FGM coatings; $\sigma_0 = E_s \alpha_s \Delta T$.

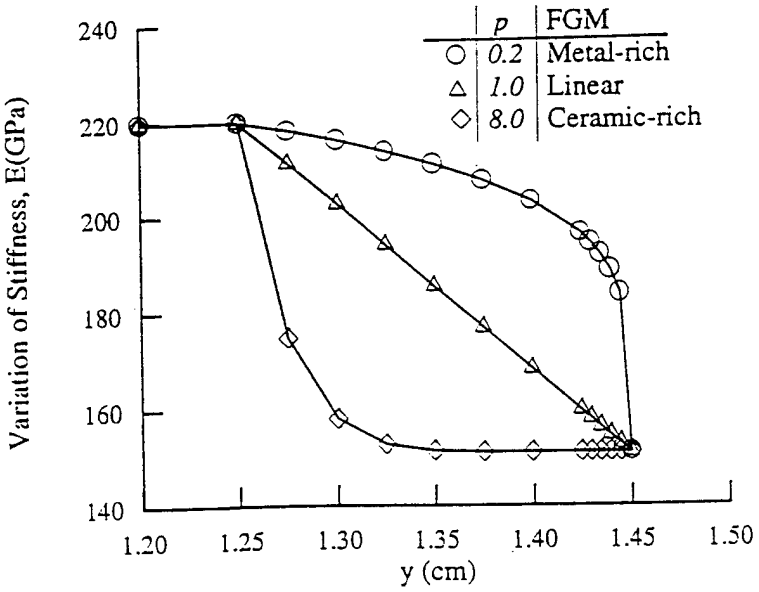

Fig. 38 Distribution of the elastic modulus E(y) for the FGM coating.